Fuentes-Fayos *et al.*
Acta Neuropathologica Communications (2025) 13:142
https://doi.org/10.1186/s40478-025-02040-w

Acta Neuropathologica Communications

RESEARCH

Open Access

Impaired splicing machinery in craniopharyngiomas unveils PRPF8 and RAVER1 as novel biomarkers and therapeutic targets

Antonio C. Fuentes-Fayos[1,2,3,4,5*†], Miguel E. G-García[1,2,3†], Teresa Sánchez-Medianero[1,3,6†], John Apps[7,8], Álvaro Flores-Martínez[1,2,3], Ana S. De la Rosa-Herencia[1,2,3], Ignacio Gil-Duque[1,2,3], Georg Otto[9], Eva Venegas-Moreno[10], Eugenio Cárdenas Ruiz-Valdepeñas[11], Aura D. Herrera-Martínez[2,3,12], Juan Solivera[2,3,13], Manuel D. Gahete[1,2,3,14], David A. Cano[10], Rosa Ortega[1,3,6], Alfonso Soto-Moreno[10], María A. Gálvez-Moreno[2,3,12*], Juan Pedro Martínez-Barberá[15] and Raúl M. Luque[1,2,3,14*]

Abstract

Craniopharyngiomas are rare benign pathologies but clinically challenging tumours because of their intimate relationship with critical brain structures, leading to severe endocrine-deficiencies/comorbidities. Therefore, identifying alternative prognostic/therapeutic tools is crucial. Although dysregulated splicing is a molecular feature that characterizes almost all tumour/cancer types, the dysregulation of the components belonging to the molecular machinery controlling the splicing-process (spliceosome) remains unknown in craniopharyngiomas. Here, we uncover a profound dysregulation in the expression of relevant spliceosome-components and splicing-factors in craniopharyngiomas versus control non-tumour tissues, identifying PRPF8 and RAVER1 as key tumour suppressor factors associated with relevant oncogenic processes. Moreover, we demonstrate that the spliceosome activity inhibition using pladienolide-B in primary patient´s derived cell-cultures might serve as a potential therapeutic tool worth to be explored in humans. Altogether, our results demonstrate a drastic and clinically relevant spliceosome-associated molecular dysregulation in craniopharyngiomas, which could serve as a potential source of novel diagnostic/prognostic biomarkers and therapeutic targets.

Keywords Craniopharyngioma, Spliceosome components, Splicing factors, PRPF8, RAVER1, Antitumour therapy, Pladienolide B

†Antonio C. Fuentes-Fayos, Miguel E. G-García and Teresa Sánchez-Medianero have contributed equally to this work.

*Correspondence:
Antonio C. Fuentes-Fayos
Antonio.Fuentes@cshs.org
María A. Gálvez-Moreno
mariaa.galvez.sspa@juntadeandalucia.es
Raúl M. Luque
raul.luque@uco.es
Full list of author information is available at the end of the article

Introduction

Craniopharyngiomas (CPs) are slow-growing (WHO grade I), rare tumours of the Central Nervous System (CNS) that constitute approximately 1.2–4.6% of all intracranial tumours, with an estimated incidence of 0.5–2 cases per million people and year [1]. Despite their common origin in the Rathke's pouch/craniopharyngeal duct, the last WHO classification of CNS tumours has recently recognized two separate types of CPs: adamantinomatous (ACPs; representing a 90% of the CPs, and 5–11% of intracranial tumours in children) and papillary (PCPs; representing a 10% of CPs, and present almost exclusively in adults) [2–5]. These two tumour groups, show differences in demographic, age distribution, radiological, molecular, and histological features. *CTNNB1* mutations (mostly located in exon 3) are mainly found in ACPs, while *BRAF* mutations (mainly V600E) are detected in PCP [3, 6–8]. ACPs usually show cords, lobules, and cystic cavities, as well as irregular trabeculae bordered by palisaded columnar epithelium, whilst PCPs exhibit non-keratinizing mature squamous epithelium covering fibrovascular cores [3]. Both ACP and PCPs can be clinically aggressive by compression or invasion of normal pituitary tissue, optic chiasm, optic nerves, and hypothalamus, leading to visual impairment, endocrine deficiencies, and hypothalamic syndrome, which significantly reduce the quality of life of patients and resulting in premature death [2].

Diagnosis, prediction of pharmacological response, and treatment strategies for CPs are severely limited, with surgery being the first line of treatment [2]. Furthermore, given the invasive nature of these tumours, very aggressive treatments (radiotherapy and/or proton beam therapy) are also often required, impacting patients' quality of life and shortening life expectancy [2, 9]. Therefore, the identification of new molecular diagnostic and/or prognostic markers, to better define their tumour behaviour, and especially novel therapeutic molecular targets is necessary and urgently needed to combat this devastating tumour pathologies.

Several tumour pathologies, including those of the CNS, are known to share atypical presence, alteration or loss of relevant components of key molecular machinery regulating cell pathophysiology. Among these dysregulations, the splicing process has been recently reported as a recurrent hallmark in neoplasias [10–14]. Splicing consists of the intricate nuclear processing of precursor mRNA (pre-mRNA) transcripts into a mature mRNA after the removal of introns and the junction of exons [15, 16]. This process is carried out by the spliceosome, a macromolecular machinery formed by several RNA–protein subunits which constitute the core component, differentiating between major or minor spliceosome (U2-dependent and U12-dependent, respectively) [16–19]. This core is tightly coordinated with a wide variety of proteins, the splicing factors (SFs), which specifically regulate the processing of > 90% of total coding genes in humans [16]. Therefore, since splicing is a physiological process that contributes to increasing genomic versatility, it is also a critical biological event in pathological conditions [20]. Indeed, alterations in the splicing process have been reported as a crucial tumour characteristic, leading to the appearance of dysregulated spliceosome components (SCs), SFs, and, consequently, aberrant splicing variants (SVs) generated by alternative splicing. These variants are associated with the initiation, development, progression, and aggressiveness in various types of cancer including bladder [21], pancreas [22], breast [23, 24], prostate [25–27], hepatocarcinoma [28–30], oral [31], pituitary [32], and brain (e.g., glioblastoma [33, 34]).

Consequently, a better understanding of the regulation of splicing in normal versus tumour tissues may help identify novel diagnostic and prognostic biomarkers and therapeutic tools to target tumour pathologies. An SV of *TP63* gene (ΔNp63), previously associated with other tumour pathologies [35, 36], is the only SV reported so far in CPs [37], but authors did not deepen into the relevance of this SV in the physiopathology of CPs. In a proteomic study, comparing ACPs with PCPs has shown the overrepresentation of RNA splicing process in ACPs, including the upregulation of several SFs such as CSTF1, SNRPF, RTRAF, and HNRNPU [38]. However, no studies have reported to date a comprehensive analysis to ascertain whether the splicing machinery (major or minor spliceosome components, and their auxiliary SFs) is altered in CPs. Moreover, the functional role associated with this potential dysregulation of the spliceosome has not yet been characterized in CPs, nor its potential therapeutic value.

In this study, we have analysed the expression profile of a representative set of key spliceosome components and SFs and their relationship with critical clinical and molecular features of CP patients using well-characterized cohorts of human CPs. In addition, we have investigated the functional role and therapeutic potential of the most critical components identified within the spliceosome machinery in CPs.

Results

Splicing machinery is dysregulated in ACP and PCPs

The expression levels of the components of the splicing machinery (SCs and SFs) were initially and simultaneously analysed using a dynamic qPCR microfluidic custom-made array in 27 ACPs, 4 PCPs and control tissues [11 normal pituitaries (NPs) and 4 brain samples (NBs)] (Table 1).

Table 1 Demographic and clinical parameters of cohort-1 of patients with craniopharyngiomas [ACPs ($n=27$) and PCPs ($n=4$)] included in this study

Parameters	Control donors		ACP patients	PCP patients
Internal Cohort	**NP**	**NB**		
Patients (*n*)	11	4	27	4
Gender (M/F)	6 (54.55%)/5 (45.45%)		13 (48.14%)/14 (51.86%)	1 (25.00%)/3 (75.00%)
Mean age at surgical intervention (range)	61 (44–85)	51.3 (45–58)	31.15 (3–63)	43.25 (10–68)
Recurrence	–	–	13 (48.15%)	2 (50%)
%KI67 (mean ± desvest)	–	–	9.5 ± 13.01	1 ± 0

Non-pathologic pituitary ($n=11$) and brain control-samples ($n=4$) from donors were also obtained from autopsy and craniotomy

We first analysed the results obtained in ACP. An initial non-supervised hierarchical analysis based on the expression levels of all the splicing-machinery components showed a perfect separation between ACPs and control-tissues into two independent clusters (Supplemental Fig. 1A). In fact, this analysis revealed that NPs and NBs do not separate (i.e., have similar expression profiles in the splicing-machinery components), which was also corroborated by principal component analysis (PCA; Supplemental Fig. 1B). In fact, although some but limited differences were observed in the expression levels of specific SCs/SFs when comparing pituitary versus brain normal tissues, the hierarchical heatmap and PCA analyses further confirmed an overall similar expression profile across these two normal tissue types (Supplemental Fig. 1C, D, respectively). Importantly, expression levels of *PRPF40A*, *PRPF8*, *RAVER1*, and *RBM22* (key SCs/SF identified in this study and further discussed below) were not altered when comparing pituitary versus brain normal tissues (Supplemental Fig. 1E). Therefore, further analyses were conducted comparing ACPs to NPs, as previously done [39].

We found a marked dysregulation in the expression levels of multiple components of the splicing machinery (SCs and SFs) in ACPs relative to control-NPs (42 out of 45 elements altered; Fig. 1A). Specifically, there was a significant downregulation of 15 SCs; 3 out of 4 minor SCs (*RNU6ATAC*, *RUN4ATAC,* and *RNU11*), and 12 out of 13 major SCs (*RBM22, PRPF8, PRPF40A, TCERG1, SF3B1, SF3B1 TV1, U2AF2, U2AF1, RNU6, RNU4, RNU2,* and *RNU1*). Additionally, this analysis revealed that 27 out of 28 SFs were also downregulated in ACP (*TIA1, TRA2A, TRA2B, SNW1, SRSF2-6, SRSF9-10, SRRM1, SND1, KHDRBS1, RBM45, RBM3, RBM17, RAVER1, PTBP1, SFPQ, SRRM4, NOVA1, MAGOH, ESRP2, ESRP1, CELF1,* and *CELF4*) (Fig. 1A). Non-supervised hierarchical analysis based on the expression levels of all the splicing-machinery components was also able to perfectly distinguish between ACPs and control-NPs into two independent clusters (Fig. 1B), which was also corroborated by PCA (Fig. 1C).

To explore further which factors were more relevant in differentiating between ACP and NPs, we used partial least squares-discriminant analysis (PLS-DA),

(See figure on next page.)

Fig. 1 Splicing machinery is drastically dysregulated in adamantinomatous craniopharyngiomas (ACPs). **A** Individual fold-change of each splicing-machinery component expression level in ACPs compared to normal pituitary glands (NPs). **B** Hierarchical heatmap showing expression levels of all the spliceosome components (major and/or minor) and splicing factors determined in NPs [Controls (green group); $n=11$] and ACPs samples [red group; $n=27$] from our internal cohort. **C** Principal Components Analysis (PCA) of the mRNA expression levels of the splicing-regulatory elements in the same set of samples. **D** Variable Importance in Projection (VIP) scores were obtained from Partial Least Squares Discriminant Analysis (PLS-DA) of top-selected splicing machinery components. **E** Individual mRNA expression levels from selected splicing machinery components (*PRPF40A*, *RAVER1*, *PRPF8,* and *RBM22*) in NPs and ACP tissues. **F** Receiver Operating Characteristic (ROC) curves analysis confirming the ability of *PRPF40A*, *RAVER1*, *PRPF8,* and *RBM22* to discriminate between ACPs and NPs. **G** Hierarchical heatmap showing the expression levels of the top 4 most discriminating factors. **H** Hierarchical heatmap also showing the expression levels of the top 4 most discriminating splicing-regulatory components (*PRPF40A*, *RAVER1*, *PRPF8,* and *RBM22*) in an independent cohort of in ACP and NP tissues (validation cohort: GSE94349), as well as their PCA (**I**) and PLS-DA (**J**) analyses. Individual mRNA expression levels of *PRPF8* (**K**), *RAVER1*, *PRPF40A*, and *RBM22* (**L**) in the ACPs and NPs of the validation cohort, and the ROC curve of *PRPF8* showing the accuracy to discriminate between both groups of samples (**K**). Individual mRNA expression levels of *PRPF8, RAVER1*, *PRPF40A*, and *RBM22* in the ACPs and NPs of the validation cohort, and the ROC curve of *PRPF8* showing the accuracy to discriminate between both groups of samples. Data represent the median (interquartile range). $^{**}P<0.01$; $^{***}P<0.001$, significantly different from the control (NPs) condition

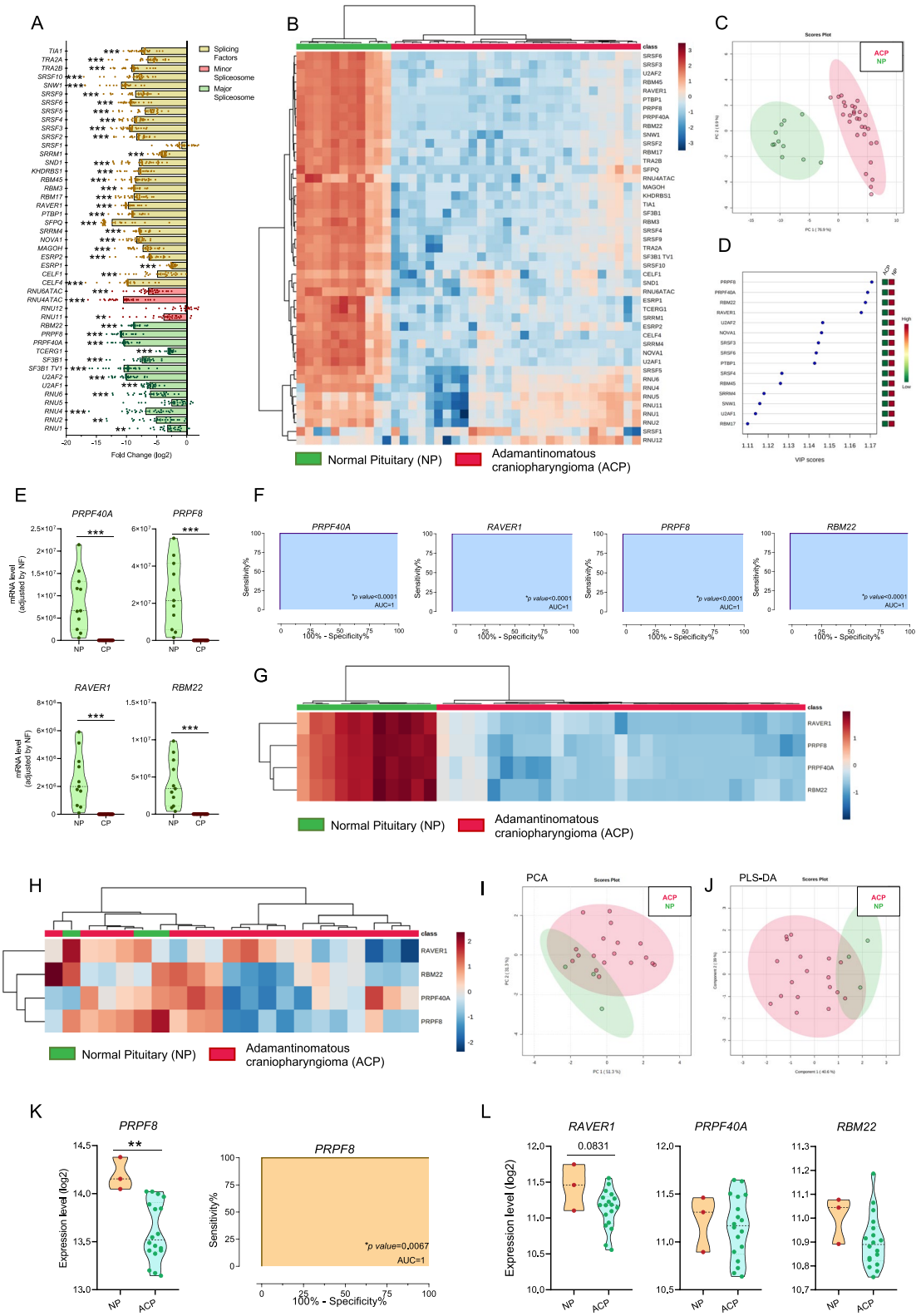

Fig. 1 (See legend on previous page.)

which revealed that 3 major SCs (*PRPF8*, *PRPF40A*, *RBM22)* and one SF (*RAVER1)* showed the highest variable importance in projection (VIP) (Fig. 1D). Specifically, expression of these four components was drastically reduced in ACPs versus control-NPs (Fig. 1E), and receiver operating characteristic (ROC)-curve analyses corroborated the capacity of these SCs/SF to finely distinguish between ACPs and controls-NPs (Area Under the Curve (AUC) of 1 ($p < 0.0001$; Fig. 1F). Moreover, as depicted in Fig. 1G, the heatmap generated with only these four SCs/SF perfectly separated ACPs from control-NPs, segregating them into two clusters.

To further validate these findings, we analysed the alterations in the expression levels of these splicing machinery components in ACPs using a second cohort of ACP samples (validation cohort) from Apps et al., 2018 [39]. Although the heatmap generated with the expression levels of *PRPF40A*, *RAVER1, PRPF8,* and *RBM22* did not completely segregate ACPs and control-tissues (Fig. 1H), PCA (Fig. 1I) and PLS-DA (Fig. 1J) analyses showed a separation of these tissues. Analyses of these 4 splicing machinery elements individually revealed no alterations in *PRPF40A* and *RBM22* expression levels between ACPs and NP controls (Fig. 1K–L). In contrast, *PRPF8* expression levels were significantly reduced in ACPs versus control-NPs (Fig. 1K). In fact, ROC-curve analysis corroborated again the capacity of *PRPF8* levels to finely separate ACPs from NP controls (AUC of 1 ($p < 0.0067$; Fig. 1K). Similarly, a trend for a statistically significant reduction in *RAVER1* levels was also observed ($p = 0.08$; Fig. 1L).

Finally, the expression levels of the components of the splicing machinery were also analysed and compared in a set of available PCPs versus control-NPs (Table 1). A marked reduction in the expression levels of SCs/SFs was observed in PCPs. Non-supervised hierarchical analysis based on the expression levels of all the splicing-machinery components (Fig. 2A), as well as only on the expression levels of *PRPF40A*, *RAVER1, PRPF8,* and *RBM22* (Fig. 2B), was also able to perfectly separate PCPs and control-NPs into two independent clusters. Corroborating this finding, other computational analyses including PCA (Fig. 2C) and PLS-DA (Fig. 2D) could also distinguish between these two sample groups. Similar to that found in ACPs, expression of *PRPF40A*, *RAVER1, PRPF8,* and *RBM22* was drastically reduced in PCPs versus control-NPs (Fig. 2E). Moreover, ROC-curve analyses corroborated the capacity of these SCs/SF to distinguish between PCPs and controls-NPs (AUC of 1; Fig. 2F).

Together, these data demonstrate a marked reduction in the expression levels of SCs and SFs in ACP and PCP tumours.

Protein levels of PRPF40A, RAVER1, PRPF8, and RBM22 are low expressed in human ACPs

Consistent with the results of mRNA, immunohistochemical (IHC) analyses of ACP tumours ($n = 20$) revealed low nuclear protein staining for PRPF40A, RAVER1, PRPF8, and RBM22 (representative images are shown in Fig. 3A). Specifically, the detection of these SCs and SFs exhibited heterogeneity across various compartments, encompassing cluster cells, palisading epithelium, and glial tissue, without demonstrating a discernible expression pattern across them. Specifically, IHC analyses revealed negative (score 0) or low (score 1) nuclear protein staining for PRPF40A, RAVER1, PRPF8, and RBM22 in 88%, 100%, 72%, and 27% of the ACP samples, respectively (Fig. 3B), which is in general consistent with the mRNA results previously observed.

The dysregulation of the splicing machinery is associated with relevant clinical and pathological parameters

First, we analysed whether the expression levels of *PRPF40A*, *RAVER1, PRPF8,* and *RBM22* were linked with patients' survival and tumour recurrence. No association was observed between survival status and the expression levels of these SCs/SF (Fig. 4A). In contrast, we found that *PRPF8* and *RAVER1* mRNA levels were significantly upregulated in recurrent ($n = 13$) relative to primary ACP ($n = 10$) tumours and *PRPF40A* showed a trend towards increased expression that did not reach statistical significance (Fig. 4B). Non-supervised hierarchical analysis based on the expression levels of these 4 spliceosome elements was able to segregate most of the primary and recurrent tumours into two clusters (Fig. 4B). Furthermore, ROC curve analyses showed a high, and statistically significant, separation capacity for tumour recurrence for all the selected splicing machinery elements (*PRPF40A*, *RAVER1, PRPF8,* and *RBM22*; Fig. 4C), suggesting a putative prognostic value of these elements for tumour recurrence pending further analyses. Interestingly, *PRPF8*, but not *RAVER1*, *RBM22*, or *PRPF40A*, mRNA levels were also significantly and positively correlated with the %KI67 (Fig. 4D). Moreover, *PRPF40A, PRPF8, and RBM22* mRNA levels were also correlated with the frequency of *CTNNB1* mutations (Fig. 4E). Based on all these data (in particular those shown in Fig. 4B), we selected *PRPF8* and *RAVER1* for further analyses.

Modulated/altered expression levels of PRPF8 and RAVER1 are linked with critical cancer processes, signalling pathways and survival rate in ACP cells

We next performed a GeneSet Enrichment Analysis (GSEA) using two human cohorts of patients with ACPs [validation cohort (GSE94349) and external cohort

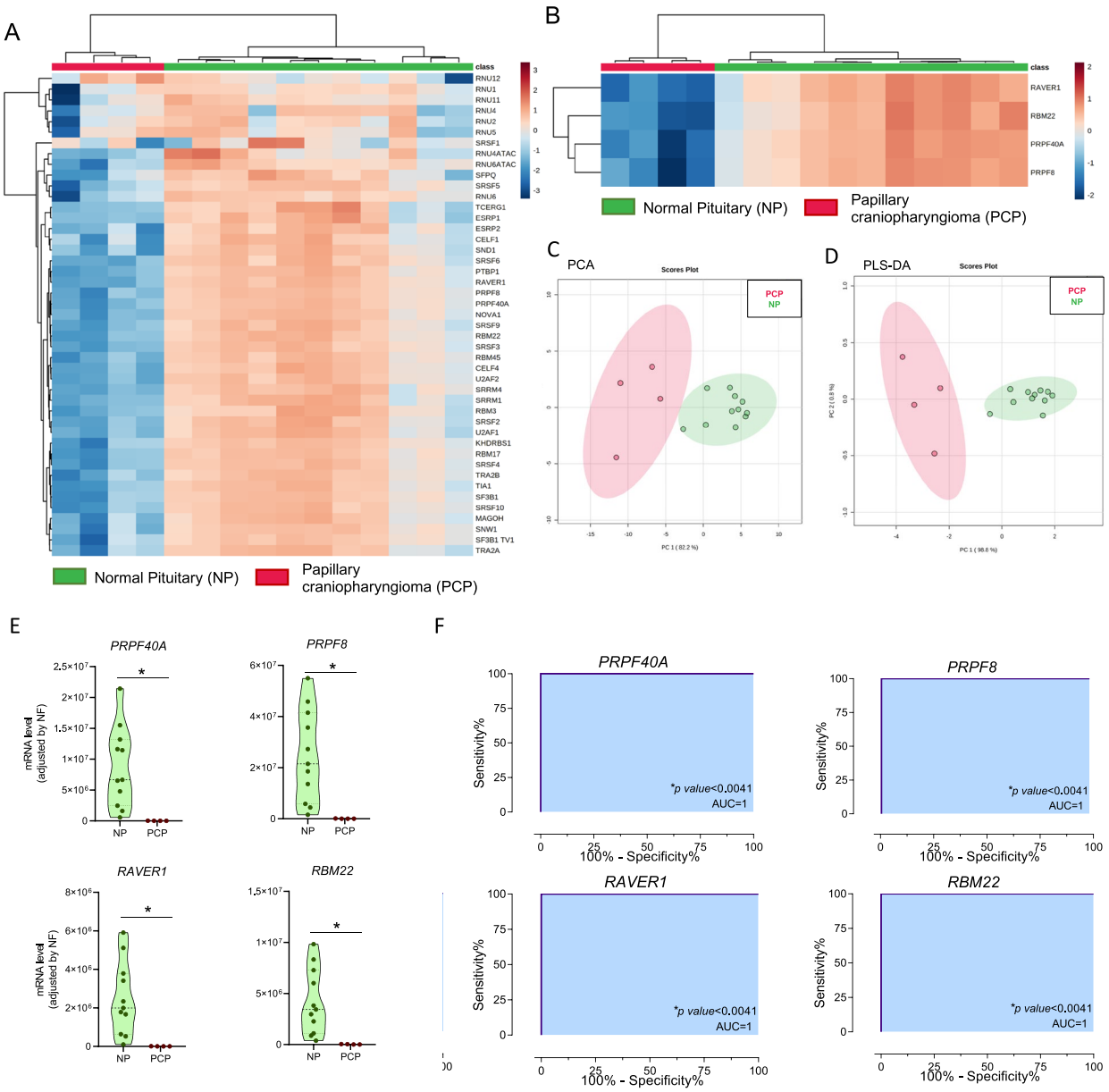

Fig. 2 Splicing machinery is also dysregulated in papillary craniopharyngiomas (PCPs). **A** Hierarchical heatmap showing expression levels of all the spliceosome components (major and/or minor) and splicing factors determined in NPs [Controls (green group); $n=11$] and PCPs samples [red group; $n=4$] from our internal cohort. **B** Hierarchical heatmap showing the expression levels of the top 4 most discriminating factors (*PRPF40A*, *RAVER1*, *PRPF8,* and *RBM22*). **C** Principal Components Analysis (PCA) and **D** Partial Least Squares Discriminant Analysis (PLS-DA) of the mRNA expression levels of the splicing-regulatory elements in the same set of samples. **E** Individual mRNA expression levels from selected splicing machinery components (*PRPF40A*, *RAVER1*, *PRPF8,* and *RBM22*) in NPs and PCP tissues. **F** Receiver Operating Characteristic (ROC) curves analysis confirming the ability of *PRPF40A*, *RAVER1*, *PRPF8,* and *RBM22* to discriminate between PCPs and NPs. Data represent the median (interquartile range). *$P<0.05$, significantly different from control tissues

(GSE68015)] and different gene databases (Hallmarks, REACTOME, and KEGG) to interrogate the molecular and pathophysiological implication of the presence of low or high expression levels of *PRPF8* and *RAVER1* in ACPs. Interestingly, we found that low expression levels of *PRPF8* and *RAVER1* were significantly linked with: (i) several key cancer-related processes [e.g., angiogenesis, epithelial-mesenchymal transition (EMT)], (ii) immunomodulatory activity (e.g., interferon signalling, interleukins signalling, inflammasomes), and (iii) the

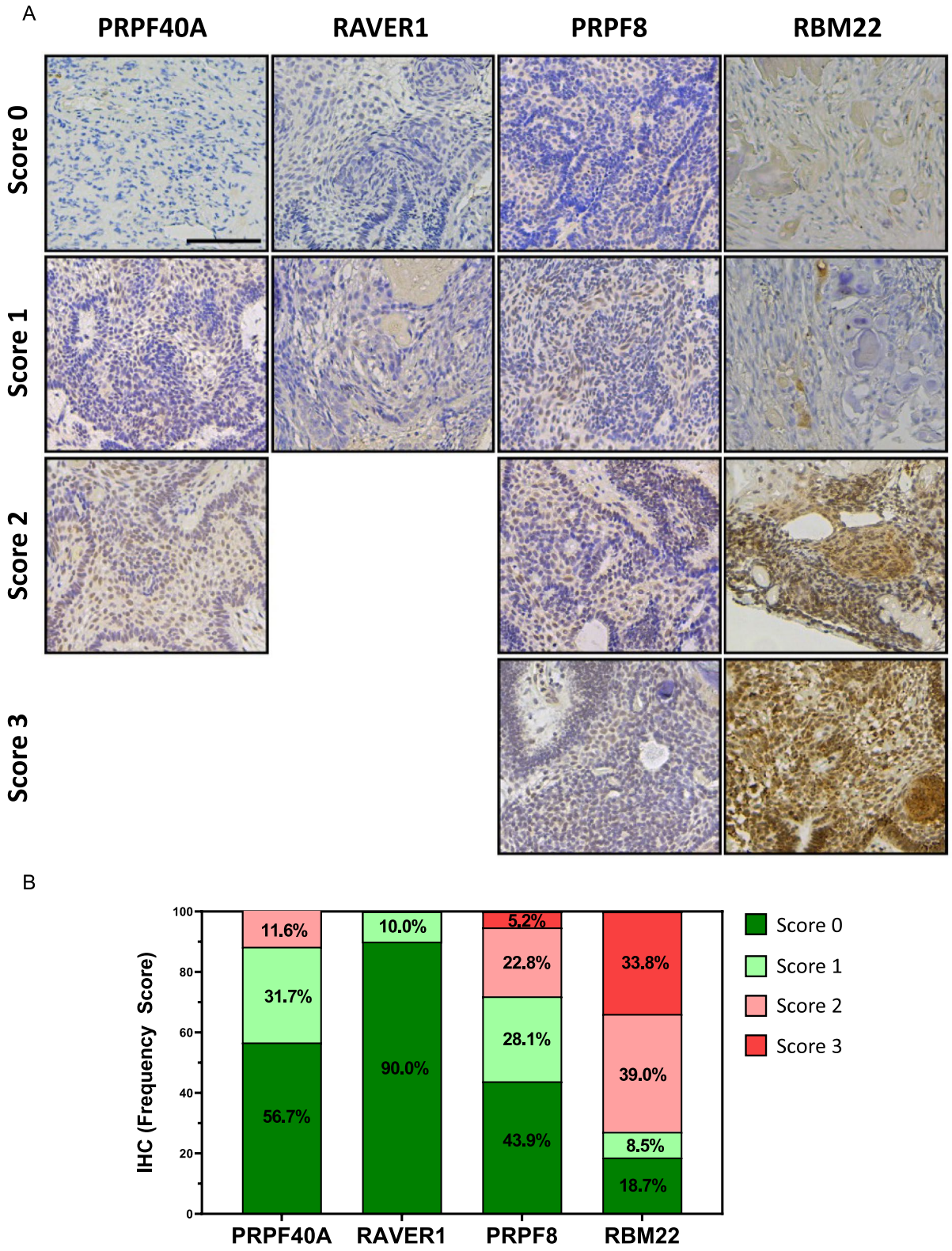

Fig. 3 Protein expression levels of PRPF40A, RAVER1, PRPF8, and RBM22 in human ACP tissues. **A** Representative images of PRPF40A, RAVER1, PRPF8, and RBM22 immunohistochemical categories in formalin-fixed paraffin-embedded (FFPE) ACP tissues (Scale bar, 100 µm). **B** Percentage of ACP samples with different Immunoreactivity Scores [IRS; Score 0 (negative, IRS 0–1); Score 1 (low, IRS 2–3); Score 2 (medium, IRS 4–8); and Score 3 (high, IRS 9–12)]

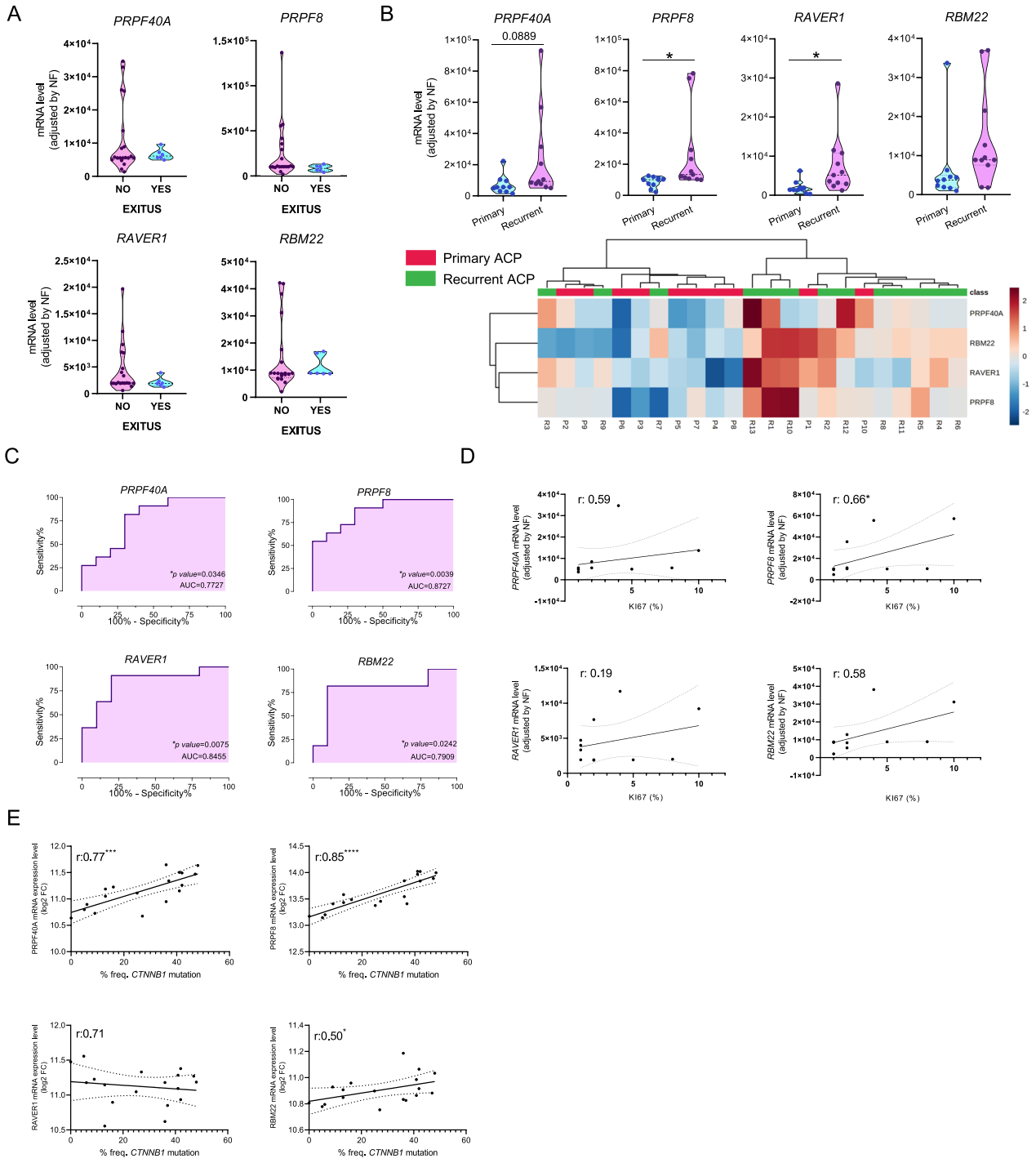

Fig. 4 The dysregulation of key splicing-regulatory elements in human CP tissues is associated with relevant clinical and pathological parameters. **A** Individual mRNA expression levels from *PRPF40A*, *RAVER1*, *PRPF8*, and *RBM22* in relation to: **A** survival status, and **B** primary versus recurrent tumours. A hierarchical heatmap and ROC curves analysis are also shown comparing primary and recurrent tumours (**B** [bottom panel; 10 primary (red group) and 13 recurrent (green group) tumours] and **C**, respectively]. Data represent median (interquartile range), and Spearman was used as a correlation test. **D)** Correlation of *PRPF40A*, *RAVER1*, *PRPF8*, and *RBM22* expression levels and %KI67 positive cells. Spearman test was performed. **E** Correlation of *PRPF40A*, *RAVER1*, *PRPF8*, and *RBM22* expression levels with the frequency of *CTNNB1* mutations in patients with CPs. Spearman test was performed. **P* < 0.05, ****P* < 0.001; *****P* < 0.0001, indicate significant differences between groups or in the analysis performed

modulation of relevant signalling pathways (e.g., hypoxia, JAK/STAT pathway, K-ras signalling) (data from validation cohort showed in Fig. 5A, and from external showed in Supplemental Fig. 2A; details in Table S2), while high *PRPF8*/*RAVER1* expression levels were connected with enrichment of different relevant processes (e.g., MYC targets, WNT/β-catenin and Hedgehog signalling) (Fig. 5A; Supplemental Fig. 2A; Table S2).

Notably, we demonstrated that in vitro overexpression of *RAVER1* and *PRPF8* (validation showed in Supplemental Fig. 2B) significantly reduced the survival rate in primary ACP-derived cell cultures (Table 2) compared to mock-control ACP cells at 24-, 48- and/or 72 h (Fig. 5B). In line with this, alterations in the expression levels of some key molecular factors associated with oncogenic processes relevant in CP physiopathology seem to occur in response to *PRPF8*-overexpressing and *RAVER1*-overexpressing in primary ACP cell cultures [i.e., upregulation of CDH1 (a negative epithelial/mesenchymal transition-EMT marker [40]) and SOCS2 (inhibitor of JAK/STAT signalling [41]), and downregulation of VIM (positive EMT marker [42]), C-MYC (proliferative oncogenic marker [43]), and EPAS1 (hypoxia marker [44])] (Fig. 5C).

In support of the previous data, phosphorylation analyses of proteins belonging to relevant oncogenic pathways of ACP cells revealed the potential involvement of different molecular pathways in the observed actions of PRPF8 and RAVER1 in primary ACP cell cultures (Fig. 5D, and Supplemental Fig. 2C). Specifically, we observed clear hyperphosphorylation of proteins belonging to the MAPK pathway [especially in *RAVER1*-overexpressing condition (CREB, ERK1-ERK2, HSP27, JNK, MEK, MKK3, MMk6, MSK2, MAPK14, TP53, RPS6KA1, and RPS6KA3), and in a lesser extend in *PRPF8*-overexpressing cells (i.e., CREB, JNK, MEK, MMk6, and RPS6KA1)], as well as proteins belonging to the AKT pathways (i.e., AKT, AMPK, BAD, EIF4EBP1, GSK3A, GSK3B, MTOR, CDKNB1, P70S6K, PDK1, PRAS40, PTEN, RAF1 and RPS6 in both *RAVER1*-overexpressing and *PRPF8*-overexpressing cells) (Fig. 5D; Supplemental Fig. 2C–D). Moreover, a slight overall decrease of phosphorylation levels in key players of the JAK/STAT (i.e., SHP1 and JAK2 in *RAVER1*-overexpressing cells; and, SHP1, JAK2, EGFR, STAT3 in *PRPF8*-overexpressing cells), NF-kB (i.e., ATM and HDAC2 in *RAVER1*-overexpressing cells; and, ATM, HDAC2, TBK1, and ZAP70 in *PRPF8*-overexpressing cells), and TGFβ (i.e., ATF2, SMAD1 and SMAD4 in *RAVER1*-overexpressing cells; and, FOS and JUN in *PRPF8*-overexpressing cells) pathways was also observed (Fig. 5D; Supplemental Fig. 2C).

The splicing pattern is different in ACPs compared to non-tumour samples

Through bioinformatic tools, splicing events were compared in ACP samples versus non-tumour control-samples (Fig. 6). Specifically, Alternative First Exon (AF) and Skipping Exon (SE) were the events more differentially produced, followed by Alternative 3´ splice site (A3), Alternative 5´splice site (A5), and Retention Intron (RI), and in the lowest proportions Alternative Last Exon (AL) and Mutually Exclusive Exons (MXE) (Fig. 6A). Enrichment analysis from alternatively spliced genes comparing ACPs versus non-tumour control-samples revealed different biological processes, highlighting endocytic pathways (Clathrin-mediated Endocytosis Signalling, SNARE Signalling Pathway), regulation of EMT, and immunomodulation (Natural Killer Cells, Granulocyte Adhesion, etc.) (Fig. 6B). Additionally, two different

(See figure on next page.)

Fig. 5 Alteration in RAVER1 and PRPF8 expression levels could be patho-physiologically relevant in CPs. **A** GSEA analysis was carried out in Hallmarks, REACTOME, and KEGG gene set databases clustering into high and low *RAVER1* (top panel) and *PRPF8* (bottom panel) expression levels and the most relevant altered pathways are shown using ACP samples from the validation cohort (GSE94349). Statistical threshold FDR < 0.25. **B** Cell survival of primary ACP-derived cells in response to RAVER1-overexpression or PRPF8-overexpression compared to mock-transfected cells (control; indicated as a dotted line at 100%) [24, 48, and 72 h]. Data represent means ± SEM. *$P < 0.05$; **$P < 0.01$, significantly different from control (mock-transfected cells) condition. **C** Individual expression levels of key oncogenic markers in ACP-derived cells ($n = 3$; *CDH1, SOCS2, VIM, C-MYC, EPAS1*, and *VEGFA*) in response to RAVER1-overexpression or PRPF8-overexpression compared to mock-transfected cells (control; indicated as a dotted line at 100%). Data represent means ± SEM. *$P < 0.05$; **$P < 0.01$, significantly different from control (mock-transfected cells) condition. **D** Left panel: Membranes of the phosphoprotein array showing the circle spots (phosphorylation levels) quantified of 5 oncogenic signalling pathways (MAPK, AKT, JAK/STAT, NF-kB, and TGFβ pathways; 55 phosphorylated proteins) in response to RAVER1-overexpressing or PRPF8-overexpressing primary ACP-derived cells and mock-transfected ACP cells (control) [ACP-derived patient cells lysates (1/3 dilution) from 3 pooled-patients per condition per group]; Top right panel: Log2 (Fold Change) of individual phosphorylation protein levels in response to RAVER1-overexpressing or PRPF8-overexpressing primary ACP-derived cells compared with mock-transfected ACP cells (control) [threshold: $\log_2(FC) = 0.2$, as previously reported[103]]; Bottom right panel: Heatmap showing the fold-change mean corresponding to each pathway in response to RAVER1-overexpressing or PRPF8-overexpressing primary ACP-derived cells and mock-transfected ACP cells (control) Membranes were incubated with blocking buffer at 25 °C for 30 min and then incubated overnight at 4 °C with 1 mL of primary ACP-derived patient cells lysates (1/3 dilution) from 3 pooled-patients per condition [Mock (Negative Control), PRPF8 and RAVER1 overexpressed cells]

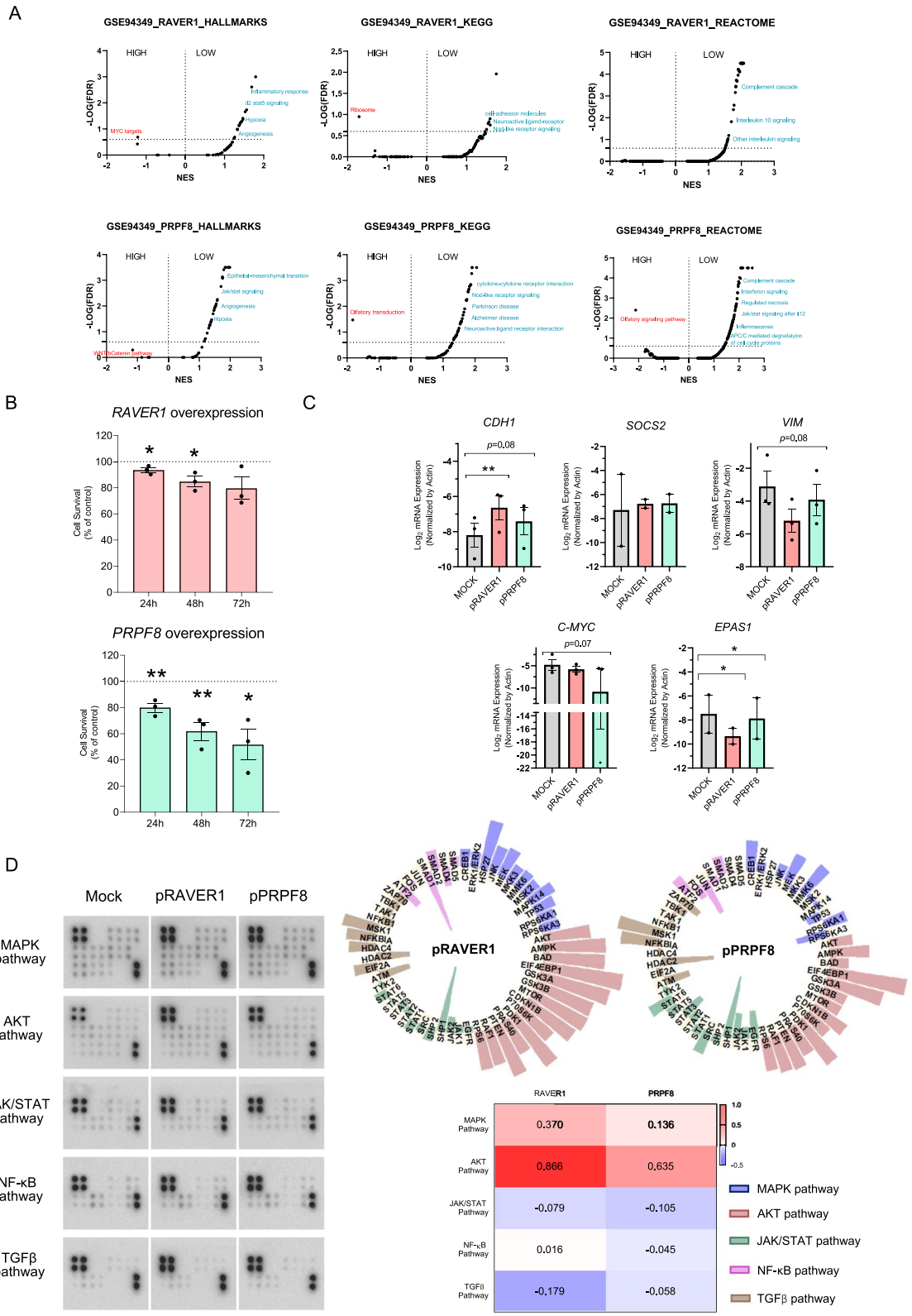

Fig. 5 (See legend on previous page.)

Table 2 Demographic parameters of the craniopharyngiomas samples (all ACPs) used to obtain primary ACP-derived cell cultures

Parameters	Experiments	
	PRPF8/RAVER1 overexpression	Pladienolide B treatment
Patients (*n*)	3	5
Gender (M/F)	2 (66.66%)/1 (33.33%)	2 (40.0%)/3 (60.0%)
Mean age at surgical intervention (range)	57.3 (34–70)	53.4 (34–70)
Histological type (Adamantinomatous/Papilar)	3 (100%)/0 (0%)	5 (100%)/0 (0%)

bioinformatic algorithms (SUPPA2 and EdgeR—see methods) were used to identify splicing processes alternatively produced between ACPs and non-tumour control-samples which revealed 93 differentially spliced genes with the SUPPA2 and 267 spliced genes with EdgeR tools (Fig. 6C; details in Table-S3). Remarkably, 22 spliced genes resulted to be common across both bioinformatic algorithms (Fig. 6C; Table S3; Supplemental Fig. 3A), wherein an enrichment in clathrin/reelin/immune system processes was found (Fig. 6D). Interestingly, specific markers relevant in CP pathophysiology (*i.e., AXIN2*, *BMP4*, *SHH*, etc. [39, 45, 46]) showed also dysregulations in delta Percent Spliced In (dPSI) comparing splicing events in ACPs and non-tumour control samples (Supplemental Fig. 3B).

Pharmacological inhibition of the splicing machinery reduces survival rate of ACP cells

As a proof of concept of the previously observed data indicating that the alteration of the splicing machinery could be pathophysiological relevant in CPs, we evaluated the effect of the pharmacological inhibition of the splicing machinery using pladienolide B [10^{-7} M; an inhibitor of the activity of the splicing-factor-3B-subunit-1 (SF3B1), a core spliceosome component] in the survival rate of primary ACP cell cultures [Fig. 7; dose selected by dose–response experiments (Supplemental Fig. 4)] which revealed a significant decrease in the survival rate at 48 and 72 h.

Discussion

CPs are slow-growing and rare tumours of the CNS (WHO grade I) that constitute approximately 1.2–4.6% of all intracranial tumours (incidence of 0.5–2 cases per million people per year) [1], which have been recently classified as ACPs and PCPs tumour types, differentiated based on distinct demographic, radiological, and histopathological features, as well as genetic alterations (i.e., *CTNNB1 vs. BRAFV600E* mutations, respectively) and profiles of methylation [3, 47]. Although histologically benign, both types of CPs exhibit aggressive clinical behaviour, including compression of normal pituitary tissue, optic chiasm, and optic nerves, which can lead to severe endocrine deficiencies and comorbidities and/or visual impairment which drastically worsen notably the quality of life of patients [3, 6, 47]. Moreover, diagnosis based on MRI, prognostic factors, and, especially, therapeutic options for CPs are very limited and typically involve surgery as the first line of treatment, where resection cannot be frequently completed causing high recurrence rates [2]. Furthermore, given the invasive nature of some of these tumours, very aggressive treatments (radiotherapy and/or proton beam therapy) are often required, which again can significantly impact patients' quality of life and reduce life expectancy [9]. Thus, the identification of new molecular diagnostic, prognostic, and therapeutic tools enables us to refine their detection, define tumour behaviour (from tumourigenesis to progression behaviours), and develop new treatments deemed crucial to combat these devastating tumours.

In this context, accurate pre-mRNA splicing is essential for proper protein translation; however, dysregulated RNA splicing is a molecular feature that characterizes almost all tumour/cancer types, in which cancer-associated splicing alterations can arise from both recurrent mutations and altered expression of factors governing splicing catalysis and regulation [13]. Thus, the splicing process is regulated and carried out by the spliceosome, a macromolecular machinery comprised of a combination of multiple spliceosome components and splicing factors, wherein defects in this molecular machinery have been related to the initiation, progression, and/or aggressiveness of different tumours/cancer types, including several intracranial tumours (glioblastoma [33], meningiomas [48], pituitary tumours [32], etc.), and other tumour pathologies [21, 23, 24, 30, 49–54]. Here, we demonstrate for the first time a drastic dysregulation in the expression profile of the components belonging to the splicing machinery (SCs and SFs) in a well-characterized cohort of ACPs and PCPs as compared to control non-tumour tissues (NPs and/or NBs), wherein most of the SCs and SFs were markedly downregulated. Indeed, numerous alterations in the expression of SCs/SFs were found in CPs versus control samples compared with the more limited tissue-specific alterations found in non-tumour samples (brain versus pituitary comparison) suggesting that a global spliceosome dysregulation might be a

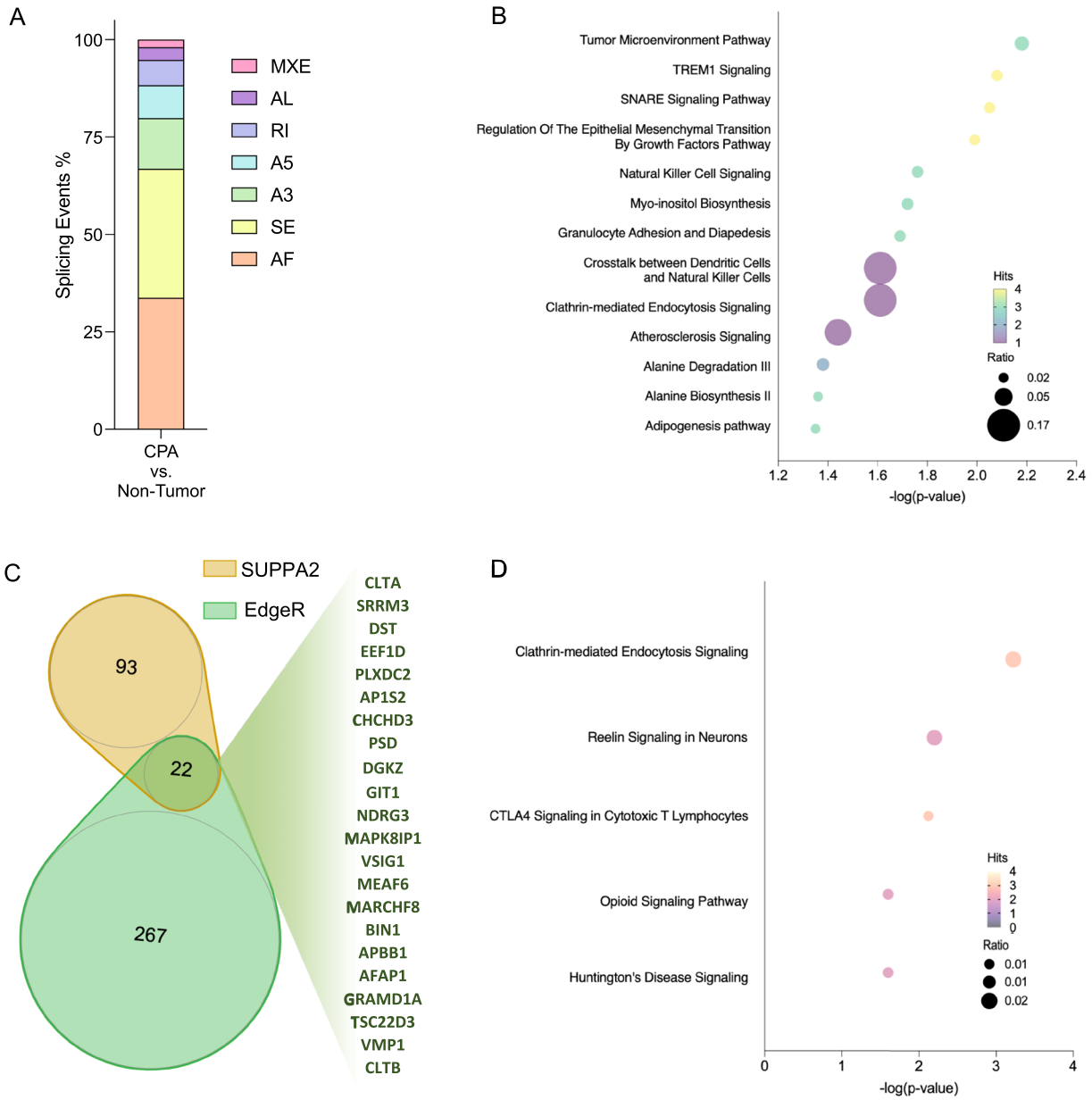

Fig. 6 Alterations in the splicing process in ACPs and potential functional relevance. **A** Percentage of altered splicing events in ACPs versus non-tumour samples (MXE: Mutual Exclusive Exon; AL: Alternative Last Exon; RI: Retained Intron; A5: Alternative 5´donor site; A3: Alternative 3´acceptor site; SE: Skipped exon; AF: Alternative First Exon). **B** Enrichment analysis from alternatively spliced genes sorted by -log(p-value). Hits (colour of circles) represent the number of alternatively spliced genes which are comprised in each depicted geneset on the Y-axis. Ratio (size of circles) represents the proportion of these alternatively spliced genes in each gene set. **C** A significant number of genes with alterations in their splicing process were identified by Suppa2 (yellow) and EdgeR (green) algorithms. The 22 common spliced genes across both bioinformatic algorithms are indicated. **D** Enrichment analysis from 22 common genes identified simultaneously by Suppa 2 and EdgeR algorithms sorted by -log(p-value). Hits (colour of circles) represent the number of alternatively spliced genes which are comprised in each depicted geneset on the Y-axis. Ratio (size of circles) represents the proportion of these alternatively spliced genes in each geneset

molecular hallmark commonly observed across different cancer types when compared with their associated control-tissues. In fact, bioinformatics analyses defined an expression-based molecular fingerprint of these SCs/SFs able to perfectly discriminate between ACPs or PCPs versus control tissues, which further reinforces the idea

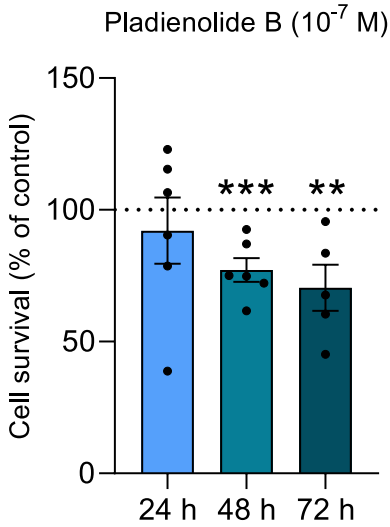

Fig. 7 Inhibition of the activity of the splicing machinery reduces survival rate of primary ACP cell cultures. Cell survival in response to pladienolide B at 10^{-7} M in primary ACP-derived cells ($n = 5$), measured by resazurin reduction. Data represent means ± SEM. $^{**}P < 0.01$; $^{***}P < 0.001$, significantly different from controls (vehicle-treated cells)

that CPs curse with a global splicing dysregulation, as we have previously reported in other tumour pathologies [22, 23, 29, 30, 33, 53–55].

Substantiating this idea by evidence, we demonstrated that differential splicing events were found in ACPs as compared with non-tumour samples. Specifically, alternative First Exon, Skipping Exon, and alternative 3´ acceptor site were the most differential splicing events found in ACPs, being these events previously associated with the malignancy of specific tumours [56–58]. These altered splicing events, possibly produced (at least in part) by the drastic dysregulation in multiple molecular elements of the splicing machinery controlling the splicing process, could potentially drive the generation of splicing events/variants of 22 alternatively spliced genes identified in the present study in ACPs. Notably, these 22 alternatively spliced genes were associated with endocytosis, inflammatory events, reelin signalling (associated with EMT and inflammation processes in brain tissue [59]), etc., and some of them (i.e., *CLTA* [60], *SRRM3* [61], *NDRG3* [62], *VSIG* [63], *PLXDC2* [64], *MARCHF8* [65], *DGKZ* [66], and *GIT1* [67]) have been widely reported as relevant factors in several tumour types (hepatocarcinoma [60], neuroendocrine prostate cancer [61], gastric cancer [62], head and neck tumours [64, 65], breast cancer [66, 67]), remarking the potential clinical value and pathophysiological relevance of the results reported herein in CPs. Additionally, mean dPSI of specific splicing event types also revealed a clear splicing alteration in key markers associated with CP pathophysiology when comparing CP versus non-tumour samples, highlighting the sonic hedgehog (SHH), a signalling pathway whose pathogenic role has been previously reported in medulloblastoma [68].

Interestingly, further clustering analysis performed in our internal cohort of ACP samples revealed that *PRPF40A*, *PRPF8*, *RAVER1*, and *RBM22* were the splicing elements with higher capacity to discriminate between ACP samples and control samples. Specifically, the expression levels of these elements were drastically reduced in ACPs versus NPs, and importantly, this alteration and discriminatory capacity of these elements were also observed in PCPs compared to NPs and similarly confirmed for *RAVER1*, and especially for *PRPF8*, in an independent validation cohort of ACPs. However, results with PCP samples should be interpreted with caution given the limited number of patients available for these studies (*i.e.,* PCPs accounted for only 10% of cases of all CPs) [5]. Notably, we also evidenced an overall low protein level of PRPF40A, PRPF8, and RAVER1, whereas RBM22 protein levels displayed a more homogeneous proportion in ACP tissues. Unfortunately, IHC analyses could not be performed in PCPs given the limited availability of samples to perform this analysis.

Then, we analysed the potential implication of the alteration of *PRPF40A*, *PRPF8*, *RAVER1*, and *RBM22* in the pathophysiology of ACPs. Specifically, our data may highlight a putative prognostic value of tumour recurrence (a critical clinical problem in CPs [69]) for *PRPF8* and *RAVER1* since their levels were upregulated in recurrent versus primary tumours. In this context, we might hypothesise that this upregulation in the expression levels of *PRPF8* and *RAVER1* observed in recurrent tumours (closer to non-tumour samples) might be associated with radiotherapy treatment received by these patients as it has been reported to influence changes in transcription and splicing process of multiple genes [70, 71]. Interestingly, *PRPF8*, but not *RAVER1*, mRNA levels were also significantly and positively correlated with the %KI67 (a well-known tumour prognosis marker [72]), and with the frequency of *CTNNB1* mutations, which further supports the prognostic value of *PRPF8*. In fact, the association between *PRPF8* and the frequency of *CTNNB1* mutations could be clinically relevant since ACPs are driven by somatic mutations in *CTNNB1* (encoding β-catenin) that affect β-catenin stability wherein mutated β-catenin cannot be efficiently degraded, leading to its nuclear accumulation and the activation of Wnt signalling pathway, which is critical for ACP development [3, 6–8]. Based on these and the previous results, *PRPF8* and

RAVER1 were selected to perform further functional and molecular studies.

Actually, we found that *PRPF8* and *RAVER1* directly associate with ACP cells aggressiveness. Specifically, the overexpression of both elements in primary ACP cell cultures decreased their survival rate and also altered the expression of genes involved in relevant tumour processes such as the EMT (i.e., *CDH1* and *VIM*) [40, 42], proliferation (i.e., *MYC*, which is also a target gene from β-catenin/WNT pathway) [43, 73, 74], and hypoxia (i.e., *EPAS1*) [44]. This result could contradict our previous findings on the correlations between PRPF8 and RAVER1 with %KI67, suggesting that the role of %KI67 in the tumour may extend beyond proliferation [75–77]. In addition, *PRPF8* and *RAVER1* have been associated with certain tumour pathologies (breast, liver, lung, ovarian and pancreatic cancers, myeloid neoplasms, and glioblastoma) [29, 54, 78–81], to the best of our knowledge, this is the first report identifying a relevant functional role of these splicing machinery elements in human CPs. In support of these findings, GSEA analysis revealed an enrichment of JAK/STAT signalling pathway in ACP samples with low mRNA levels of *PRPF8* and *RAVER1*, a signalling pathway that has been previously reported as constitutively hyperactivated in brain tumours [82–85]. Additionally, low expression levels of PRPF8 and/or RAVER1 were also associated with general hallmarks of cancer, such as hypoxia (related to the increased levels of HIF-1α in ACPs [86]), angiogenesis (even considered as a prognostic factor in CP [87, 88]), EMT (relevant in CP progression through VIM, cadherin, and β-catenin markers [89, 90]). Even more, the previous analyses of differential splicing events also suggested a potential link between low levels of PRPF8 and/or RAVER1 and the previously reported increase in immune infiltration observed in both ACPs and PCPs [91, 92], since low levels of these splicing elements were associated with inflammatory response, cytokine interaction, and inflammasome events. In this sense, it has been reported that interleukin-6 (enriched in low *PRPF8* expression level samples) is capable of inducing an EMT phenotype in ACP cells and promotes tumour aggressiveness [93] and also could act as a tumour inductor associated with inflammation in CPs [94].

Next, to interrogate the signalling mechanisms underlying the pathophysiological role of *PRPF8* and *RAVER1* in CPs, we explored an ample range of cancer-related signalling pathways in response to *PRPF8* and *RAVER1* overexpression in primary ACP cell cultures. In accordance with the previously observed enrichment of JAK/STAT signalling pathway in ACP samples with low mRNA levels of *PRPF8* and *RAVER1* (GSEA analysis), a striking downregulation of JAK/STAT phosphorylation levels was observed in cells overexpressing *PRPF8* (through the decrease of SHP1, JAK2, STAT3, and EGFR) as well as in cells overexpressing *RAVER1* (through SHP1 and JAK2). Additionally, *PRPF8*-overexpressed cells also exhibited a decrease in phosphorylation levels of NF-κB (through the reduction of HDAC2, ATM), and the increase of NFKBIA (inhibitor of NF-κB pathway), being both pathways related to the progression of cancer including brain tumours [83, 84, 95]. Similarly, a downregulation in the phosphorylation levels of the TGF-β pathway (through ATF2, SMAD1, SMAD4) was also observed in *RAVER1*-overexpressed cells which have been associated with the development of certain tumour types [39, 83]. Overall, these data provide original, compelling evidence indicating that the molecular elements of the splicing machinery *PRPF8* and *RAVER1* are functionally linked to these well-known pathophysiologically relevant pro-oncogenic pathways in CPs [JAK/STAT, NF-κB and NFKBIA signalling in *PRPF8*-overexpressed cells; JAK/STAT, and TGF-β signalling in *RAVER1*-overexpressed cells], which further support the potential clinical-pathophysiological importance of the dysregulation of the splicing machinery in ACPs. In contrast, two reported pro-oncogenic pathways in CPs, the AKT and MAPK signalling routes [96, 97], were found to be hyperphosphorylated in response to PRPF8- and RAVER1-overexpression, which might suggest that PRPF8/RAVER1 overexpression could be forcing to CP cells to be more dependent on these critical pathways. Although further analyses would be necessary to clarify these unforeseen findings, we might speculate that a combined therapy between AKT/MAPK inhibitors (already purposed as a therapeutic strategy to combat CPs [39, 96]) and modulators of spliceosome PRPF8/RAVER1 actions may perhaps be a therapeutic option worth to be tested in the future.

As a matter of fact, our study provides an initial, unprecedented proof-of-concept on the suitability of splicing dysregulation as a novel potential target for CP treatment by demonstrating that the pharmacological impact of inhibiting the splicing process has significant beneficial consequences in ACP cells. Specifically, we tested the direct effects of pladienolide-B in primary ACP cell cultures which demonstrate, for the first time, that the inhibition of the spliceosome activity significantly inhibited cell survival in primary ACP cell cultures, which compares well with recent data from our group showing that pladienolide-B reduced proliferation rates in the pituitary, brain, prostate, liver, pancreas, and oral tumours [26, 31, 32, 34, 98, 99].

Taken together, our results unveiled new conceptual and functional avenues in CPs, with potential therapeutic implications, by demonstrating for the first time a drastic dysregulation of the splicing machinery in CPs. This

is likely relevant clinically, because the dysregulation of some of these spliceosome elements, especially PRPF8 and RAVER1, directly associates with tumour recurrence and the frequency of *CTNNB1* mutations, supporting not only their diagnostic value but also a prognostic capacity. Moreover, we unveil the role of PRPF8 and RAVER1 in crucial pathophysiological processes of CPs, including cell survival and key oncogenic processes such as EMT, and likely mediated through the modulation of critical oncogenic signalling pathways (i.e., JAK/STAT). Finally, our data highlight the inhibition of the activity of the splicing machinery as a putative pharmacological target in CPs, offering a clinically relevant opportunity worth exploring in humans. Therefore, our study provides solid, convincing evidence demonstrating the potential of the splicing machinery and the splicing process as a novel molecular mechanism to better understand CP biology and identify candidate biomarkers and actionable targets to tackle this devastating pathology.

Appendix

Star methods

Reagents

Unless otherwise indicated, reagents and products were purchased from Sigma-Aldrich (St. Louis, MO, USA). Pladienolide B was obtained from Santa-Cruz Biotechnology (CAS 445493–23–2).

Patient cohort and samples

A total of 31 tumour samples were obtained by intracranial surgery from patients previously diagnosed with CPs [adamantinomatous craniopharyngioma (ACPs; $n=27$) or papillary craniopharyngioma (PCPs; $n=4$)] from the Reina Sofia University Hospital (Cordoba, Spain) and Virgen del Rocio University Hospital (Seville, Spain) (Cohort-1; Table 1). The Andalusian Public Health System Biobank Biobank coordinated the collection, processing, management, and assignment of the biological samples used in this study, according to the standard procedures established for this purpose. Control (non-tumour) pituitary tissues ($n=11$; Table 1) and brain tissues ($n=4$; Table 1) were obtained from autopsy and craniotomy, as previously described [32]. Non-tumour brain samples were resected from Broca region, an area nearest to suprasellar region wherein craniopharyngiomas (CPs) are usually located [6]. All samples were histologically evaluated by expert pathologists to verify their diagnosis (CPs and/or normal pituitary/brain tissues) and to ensure the presence of tumours in the CP specimens. Available demographic and clinical characteristics of all patients/donors from cohort-1 were collected to carry out clinical correlations (Table 1). Recurrence was determined by the identification of a new lesion following gross total removal or regrowth of a tumour remnant during follow-up MRI neuroimaging. This study was conducted in accordance with the ethical standards of the Helsinki Declaration, of the World Medical Association, and with the approval of the Hospital Ethics Committee. Written informed consent was obtained from all individuals included in the study. Additionally, data from two different additional cohorts were also used to perform GeneSet Enrichment Analyses: One previously reported by our team [validation cohort (GSE94349); RNA-Seq data ($n=18$ ACPs, and $n=3$ non-tumour samples)] [39]; 2) microarray data from an external cohort (HG-U133plus2; $n=27$ ACPs) from GSE68015 [92] (see more details below in "Bioinformatic and statistical analysis" section).

RNA isolation, retrotranscription, real-time quantitative-PCR (qPCR), and customized qPCR dynamic array based on microfluidic technology

Total RNA from Formalin-Fixed Paraffin-Embedded (FFPE) normal and tumour samples was isolated, and DNase-treated using the Maxwell 16 LEVRNA FFPE Kit (Promega, Madison, WI, USA) according to manufacturer instructions in the Maxwell MDx 16 Instrument (Promega). Total RNA from transfected primary ACP-derived cell cultures was extracted with TRIzol® Reagent (Thermo Fisher, Waltham, MA, USA). In all cases, total RNA concentration and purity were assessed by Nanodrop One Microvolume UV–Vis Spectrophotometer (Thermo Fisher). For qPCR and microarray analyses, total RNA was retrotranscribed using random hexamer primers and the RevertAid RT Reverse Transcription Kit (#K1691, Thermo Fisher). Thermal profile and qPCR analysis to obtain absolute mRNA copy number/50 ng of sample of selected genes are reported elsewhere [32, 33].

As previously reported by our group [28, 32, 33, 55], a customized qPCR dynamic array based on microfluidic technology (#BMK-M-48.48, Fluidigm, San Francisco, CA, USA) was validated and implemented to determine and compare the simultaneous expression of 48 transcripts in 31 CPs, and in 11 and 4 non-tumour pituitary and brain samples, respectively, using the Biomark System and the Fluidigm® Real-Time PCR Analysis Software v.3.0.2 and Data Collection Software v.3.1.2 (Fluidigm). The samples were pre-amplified and treated with exonuclease I (New England Biolabs, Ipswich, MA, USA). Specific primers for human transcripts including components of the major spliceosome ($n=13$), minor spliceosome ($n=4$), associated splicing factors ($n=28$), and three housekeeping genes [β-actin (*ACTB*),

hypoxanthine–guanine phosphoribosyl-transferase (*HPRT1*), and glyceraldehyde 3-phosphate dehydrogenase (*GAPDH*) in order to calculate a normalization factor with GeNorm v.3.3 software] were specifically designed with the Primer3 software (Supplementary Table S1), as previously reported [32, 33].

Tissue microarrays (TMAs) preparation and immunohistochemical analyses

Tissue microarrays (TMAs) were prepared using FFPE tissues of CPs ($n=20$) obtained from archival sources of Cohort-1. Tumour regions of the paraffin blocks were identified by an experienced pathologist based on hematoxylin/eosin-stained sections, and cylindrical tissue cores were relocated for inclusion in the TMAs. Duplicate samples of each tissue were also included in the TMAs. Immunohistochemical analysis was performed as previously described [100]. Briefly, 5 µm TMA sections were prepared and processed by deparaffinization, rehydration, and permeabilization in 0.2% Triton X-100 in PBS using the PT Link system (Agilent, Santa Clara, CA, USA). When required, epitope retrieval was performed using Tris–EDTA buffer (pH 9) or Sodium citrate buffer (pH 6) according to the type of primary antibody. Then, the sections were blocked using 3% normal donkey serum in PBS for 45 min at room temperature. Primary antibodies were used at the following dilutions: rabbit anti-PRPF8 (1:200, ab79237; Abcam, Cambridge, UK), anti-RBM22 (1:200, ab59157; Abcam), anti-RAVER1 (1:100, PA5-60,424; Thermo Fisher), and anti-PRPF40A (1:200, ab204371; Abcam). Moreover, proliferating cells were stained by a monoclonal rabbit anti-KI67 (clone 30-9, VENTANA, Roche, 790-4286) using an automated immunostainer instrument (VENTANA, Roche, Basel, Switzerland) following the manufacturer's instructions. Negative controls were performed by replacing the primary antibody with PBS. Additionally, haematoxylin counterstaining was applied. The Ki-67 index was determined by calculating the proportion of positively stained tumour cell nuclei among the total number of malignant cells scored. For each sample, four high-power fields were randomly selected and counted (at least 500 tumour cells per sample were evaluated).

Semi-quantitative measurement of immunoreactivity for PRPF8, RAVER1, RBM22, and PRPF40A was also performed following methods previously described [25, 29]. Specifically, we used the Immunoreactivity Score (IRS) method, a widely accepted scoring system used in biomedical research combining staining intensity (0 = no staining; 1 = weak; 2 = moderate; and 3 = strong) and proportion of cell nuclei-positively stained (0 = 0%; 1 = 1–10%; 2 = 11–50%; 3 = 51–79%; and 4 = > 80%). A final classification was determined by categorizing the IRS values into four categories based on the multiplication of intensity and proportion values: 0 (negative, IRS, 0–1); 1 (low, IRS, 2–3); 2 (medium, IRS, 4–8); and 3 (high, IRS, 9–12). Bright-field images were captured using a BX-61 microscope (Olympus, Madrid, Spain).

Primary patient-derived ACP cell cultures

ACP samples were collected after intracranial surgery and immediately transported to the cell culture room in sterile cold Spinner's modified Eagle medium (S-MEM; #11,380-037, Gibco, Barcelona, Spain) complemented with 0.1% bovine serum albumin (BSA; #A2153), 0.01% l-glutamine (#G7513), 1% antibiotic–antimycotic solution (#R01510, Gibco) and 2.5% HEPES (#H3537). Then, ACP samples were dissociated into single cells following methods previously validated and described [101], using a mechanic/enzymatic protocol with 2% Collagenase IV (#17,104,019, Thermo Fisher) and 0.15% trypsin lyophilized powder (#215,240, BD Biosciences, Madrid, Spain). Cell viability was always determined by the trypan-blue dye method, excluding those with a low proportion of cells or a high presence of calcifications. The single cells were cultured onto poly-l-lysine (#P1524-25MG) tissue culture plates in a 10% foetal bovine serum (FBS; #F6765) containing Dulbecco's modified Eagle medium (DMEM) supplemented with D-valine (#06-1055-09-1A, Sartorius, Gotinga, Germany), complemented as S-MEM medium to perform functional/molecular assays. Demographic characterization of the ACP-samples used to obtain primary human sample-derived cell cultures ($n=5$) is depicted in Table 2.

Overexpression of PRPF8 and RAVER1 by specific plasmids

Pre-designed overexpression plasmids for upregulation of endogenous *PRPF8* and *RAVER1* expression levels (OHu19527C and OHu05974, GenScript, NJ, USA; respectively; 1,000 ng/mL) were individually transfected in primary patient-derived ACP cell cultures seeded in a 6-well plate (500,000 cells/well) using Lipofectamine 2000 reagent (#11,668,019, Thermo Fisher), according to the manufacturer's instructions and following methods previously described [25, 102]. Empty plasmid pcDNA3.1 was used as a negative-overexpressed control. After 48 h of transfection, cells were collected for: 1) validation of the transfection; 2) to extract proteins in order to analyse protein phosphorylation levels; or 3) seeded for measurement of survival and gene expression modulation (see all below).

Measurement of protein phosphorylation levels using pathway profiling array

A phosphorylation pathway profiling array was used [Human Phosphorylation Pathway Profiling Array C55 kit (#AAH-PPP-1-8, Raybiotech, GA, USA); Supplemental Fig. 2D], following the manufacturer's protocols and as recently reported [103, 104]. Briefly, membranes were incubated with blocking buffer at 25 °C for 30 min and then incubated overnight at 4 °C with 1 mL of primary ACP-derived patient cells lysates (1/3 dilution) from 3 pooled-patients per condition [Mock (Negative Control), *PRPF8* and *RAVER1* overexpressed cells]. Then, membranes were first incubated with Detection Antibody Cocktail at room temperature for 2 h and then with horseradish peroxidase (HRP)-labelled anti-rabbit secondary antibody at room temperature for 2 h. The signals were collected after adding ECL-reagent by ImageQuant LAS 4000 (GE Healthcare). Densitometric analysis of the array spots was carried out with ImageJ software (Protein Array Analyzer, an extension of Gilles Carpentier's Dot-Blot-Analyzer) using positive control spots as a normalizing factor.

Measurement of cell survival rate in response to PRPF8 and RAVER1 overexpression and to the inhibition of spliceosome activity

Cell survival in response to *PRPF8* and *RAVER1* overexpression as well as in response to pladienolide B treatment (an inhibitor of the spliceosome activity) was determined using Resazurin reagent (#R7017, Thermo Fisher) after seeding 10,000 primary ACP cells/well, following protocols previously validated and described [32–34]. Briefly, cells were seeded in 96-well culture plates, and serum-starved for 12–16 h in order to achieve cell cycle synchronization. Then, cell survival was measured at 0, 24, 48, and 72 h using Flex Station III (Molecular Devices, Madrid, Spain).

Bioinformatic and statistical analysis

Internal cohort data were evaluated for heterogeneity of variance using the Kolmogorov–Smirnov test. Statistical differences were assessed by t-test, Mann–Whitney U-test, or by one-way ANOVA followed by Fisher's correction exact test. qPCR microarray results were analysed by several tests, models, and hierarchical cluster algorithms, which allowed us to make an accurate assessment. Correlations were studied using the Spearman correlation test. All statistical analyses were performed using Prism software v.8.0 (GraphPad Software, La Jolla, CA, USA) except the clustering analyses which were performed with MetaboAnalyst Software v.5.0 (McGill University, Quebec, Canada). Additionally, two available cohorts were used to perform GeneSet Enrichment Analysis [GSEA, v.4.3.2: GSE94349 [39] ($n=18$ ACPs, and $n=3$ non-tumour samples); GSE68015 [92] ($n=27$ ACPs)]. These enrichment analyses were carried out identifying differentially expressed genes for Hallmarks (h.all.v2023.1), Reactome (c2.cp. Reactome.v2023.1), and KEGG (c2.cp.kegg.v2023.1) Gene Set Databases. A statistically significant cutoff for GSEA analyses was set at FDR < 0.25, a proposed cutoff by GSEA tool. For differential splicing analyses sequencing reads were mapped to the hg38 reference sequence using STARv2.5.3 [105] and kallisto v0.46.1 [106]. Alignments were processed using samtools version1.8 [107] and Picard tools version 2.21.8 (http://picard.sourceforge.net/). Aligned reads were filtered (uniquely mapping reads, and putative PCR duplicates were removed. Read summarization was done using featureCounts [108]. Expression analysis was carried out using R version 4.0.2 (R Core Team, 2020). Differential splicing was analyzed using the R packages edgeR [109] and SUPPA v2.3 [110]. delta Percent Spliced In (dPSI) was calculated as a difference between mean of PSI events in ACP samples and control non-tumour samples. In the Human Phosphorylation Pathway Profiling Array, a fold change (log2) of 0.2 was considered a significant threshold. Circle plots were implemented in R language (v.3.5) using the following packages: tidyverse, Viridis, and ggplot2. Values of $P<0.05$ were considered statistically significant. A trend for significance was indicated when p values ranged between > 0.05 and < 0.1. Data represent the median (interquartile range) or means ± standard error of the mean (SEM). **P*, 0.05; ***P*, 0.01; ****P*, 0.001, significantly different from control conditions.

Supplementary Information

The online version contains supplementary material available at https://doi.org/10.1186/s40478-025-02040-w.

Supplementary file 1
Supplementary file 2
Supplementary file 3
Supplementary file 4

Acknowledgements

We deeply thank all the patients and their families for generously donating the samples and clinical data for research purposes. Special thanks to the staff of Biobank of Andalusian Public Health System Biobank [Reina Sofia University Hospital (Cordoba node) and Virgen del Rocio University Hospital (Seville node)].

Author contributions

A.C.F.F., M.E.G.G., M.A.G.M and R.M.L. conceived and designed the project and interpreted the results. A.C.F.F., M.E.G.G., T.S.M., A.F.M., A.S.R.H., I.G.D, E.C.R.V., A.D.H.M., J.S., D.A.C., R.O., A.S.M., M.A.G.M., and R.M.L. coordinated samples collection. T.S.M., E.V.M., E.C.R.V., A.D.H.M., J.S., R.O., A.S.M., and M.A.G.M., identified and consented patients for the study. T.S.M. and R.O. developed IHC analysis and provided expertise in clinical pathology. A.C.F.F and M.E.G.G. performed the main experimental assays. A.C.F.F, M.E.G.G., J.A., G.O., J.P.M.B., and R.M.L

carried out bioinformatic analyses. A.C.F.F., M.E.G.G., T.S.M., J.A., G.O., A.F.M., J.A., D.A.C., M.D.G., M.A.G.M., J.P.M.B., and R.M.L., provided important experimental and analytical support and/or helped to discuss the results. A.C.F.F., M.E.G.G., and R.M.L. wrote the manuscript. A.C.F.F., M.E.G.G., T.S.M., J.A., A.F.M., A.S.R.H., I.G.D, G:O., E.V.M., E.C.R.V., A.D.H.M., J.S., M.D.G., D.A.C., R.O., A.S.M., M.A.G.M., J.P.M.B., and R.M.L. revised the manuscript for important intellectual content. A.C.F.F., M.A.G.M., and R.M.L. supervised the whole work. A.C.F.F., M.E.G.G., and R.M.L. verified the underlying data. All authors read, approved, and verified the final version of the manuscript.

Funding
This work was funded by Junta de Andalucía (PEER-0048–410, P20_00442, BIO-0139, 1–0034-2023, RPS24665), NIHR Great Ormond Street Hospital Biomedical Research Center, Foundation of the Spanish Society of Endocrinology and Nutrition (FSEEN), Spanish Ministry of Science, Innovation and Universities (Research-Grants: PID2022-1381850B-I00, FPU20/03954), and CIBERobn.

Availability of data and materials
Resource availability: Lead Contact. Under the need of any specific resources or reagents from this study, please feel free to reach out to the Corresponding Authors. Materials Availability: These resources are readily available upon request and will be provided. Data and Code Availability: All data and code used or created for this study are available upon request and will be provided.

Declarations

Ethics approval and consent to participate
This study was conducted in accordance with the ethical standards of the Helsinki Declaration, of the World Medical Association, and with the approval of the Hospital Ethics Committee [Reina Sofia University Hospital (Cordoba, Spain); Virgen del Rocio University Hospital (Sevilla, Spain)]. Written informed consent was obtained from all individuals included in the study.

Consent for publication
Written informed consents were obtained from all individuals included in the study enclose the use and consent for publication of data in this manuscript.

Competing Interests
The authors declare no competing interests.

Author details
[1]Maimonides Institute of Biomedical Research of Cordoba (IMIBIC), 14004 Córdoba, Spain. [2]Department of Cell Biology, Physiology and Immunology, University of Cordoba, 14004 Córdoba, Spain. [3]Reina Sofia University Hospital (HURS), IMIBIC Building. Av. Menéndez Pidal s/n, 14004 Córdoba, Spain. [4]Department of Biomedical Sciences, Cedars-Sinai Medical Center, Los Angeles, CA, USA. [5]Board of Governors Regenerative Medicine Institute, Cedars-Sinai Medical Center, Los Angeles, CA, USA. [6]Pathology Service, HURS, 14004 Córdoba, Spain. [7]UCL Great Ormond Street Institute of Child Health, University College London, London, UK. [8]Department of Cancer and Genomic Sciences, School of Medical Sciences, College of Medicine and Health, University of Birmingham, Birmingham B15 2TT, UK. [9]Genetics and Genomics Medicine, GOS Institute of Child Health, University College London, London, UK. [10]Unidad de Gestión de Endocrinología y Nutrición. Instituto de Biomedicina de Sevilla (IBiS), Hospital Universitario Virgen del Rocío/CSIC/Universidad de Sevilla, 41013 Seville, Spain. [11]Servicio de Neurocirugía, Hospital Universitario Virgen del Rocío, 41013 Seville, Spain. [12]Service of Endocrinology and Nutrition, HURS, 14004 Córdoba, Spain. [13]Service of Neurosurgery, HURS, 14004 Córdoba, Spain. [14]CIBER Physiopathology of Obesity and Nutrition (CIBERobn), 14004 Córdoba, Spain. [15]Developmental Biology and Cancer Programme, Birth Defects Research Centre, GOS Institute of Child Health, University College London, London, UK.

Received: 30 December 2024 Accepted: 13 May 2025
Published online: 28 June 2025

References

1. Ostrom QT, Patil N, Cioffi G, Waite K, Kruchko C, Barnholtz-Sloan JS (2020) CBTRUS statistical report: primary brain and other central nervous system tumors diagnosed in the United States in 2013–2017. Neuro Oncol. https://doi.org/10.1093/neuonc/noaa200
2. Apps JR, Muller HL, Hankinson TC, Yock TI, Martinez-Barbera JP (2023) Contemporary biological insights and clinical management of craniopharyngioma. Endocr Rev 44(3):518–538. https://doi.org/10.1210/ENDREV/BNAC035
3. Pedro Martinez-Barbera J, Andoniadou CL (2020) Biological Behaviour of Craniopharyngiomas. Neuroendocrinology 110:797–804. https://doi.org/10.1159/000506904
4. Hölsken A et al (2016) Adamantinomatous and papillary craniopharyngiomas are characterized by distinct epigenomic as well as mutational and transcriptomic profiles. Acta Neuropathol Commun 4:20. https://doi.org/10.1186/S40478-016-0287-6
5. Lubuulwa J, Lei T (2016) Pathological and topographical classification of craniopharyngiomas: a literature review. J Neurol Surg Rep 77:121–127. https://doi.org/10.1055/s-0036-1588060
6. Müller HL, Merchant TE, Warmuth-Metz M, Martinez-Barbera JP, Puget S (2019) Craniopharyngioma. Nat Rev Dis Primers 5(1):1–19. https://doi.org/10.1038/s41572-019-0125-9
7. Brastianos PK et al (2014) Exome sequencing identifies BRAF mutations in papillary craniopharyngiomas. Nat Genet 46(2):161–165. https://doi.org/10.1038/NG.2868
8. He J et al (2021) Characterization of novel CTNNB1 mutation in Craniopharyngioma by whole-genome sequencing. Mol Cancer 20(1):168. https://doi.org/10.1186/S12943-021-01468-7
9. Grossman A, Kosmin M (2023) Craniopharyngiomas and proton beam therapy: worth the expense? Lancet Oncol 24(5):422–423. https://doi.org/10.1016/S1470-2045(23)00162-6
10. Bonnal SC, López-Oreja I, Valcárcel J (2020) Roles and mechanisms of alternative splicing in cancer — implications for care. https://doi.org/10.1038/s41571-020-0350-x
11. Zhang Y, Qian J, Gu C, Yang Y (2021) Alternative splicing and cancer: a systematic review. Springer Nature. https://doi.org/10.1038/s41392-021-00486-7
12. Wang E, Aifantis I (2020) RNA splicing and cancer. Trends in Cancer. https://doi.org/10.1016/j.trecan.2020.04.011
13. Bradley RK, Anczuków O (2023) RNA splicing dysregulation and the hallmarks of cancer. Nat Rev Cancer 23(3):135–155. https://doi.org/10.1038/s41568-022-00541-7
14. Urbanski LM, Leclair N, Anczuków O (2018) Alternative-splicing defects in cancer: Splicing regulators and their downstream targets, guiding the way to novel cancer therapeutics. WIREs RNA. https://doi.org/10.1002/wrna.1476
15. Shi Y (2017) The spliceosome: a protein-directed metalloribozyme. J Mol Biol. https://doi.org/10.1016/j.jmb.2017.07.010
16. Ule J, Blencowe BJ (2019) Alternative splicing regulatory networks: functions, mechanisms, and evolution. Mol Cell 76(2):329–345. https://doi.org/10.1016/J.MOLCEL.2019.09.017
17. Turunen JJ, Niemelä EH, Verma B, Frilander MJ (2013) The significant other: splicing by the minor spliceosome. WIREs RNA. https://doi.org/10.1002/wrna.1141
18. Will CL, Lührmann R (2011) Spliceosome structure and function. Cold Spring Harb Perspect Biol. https://doi.org/10.1101/cshperspect.a003707
19. Yan C, Wan R, Shi Y (2019) Molecular mechanisms of pre-mRNA splicing through structural biology of the spliceosome. Cold Spring Harb Perspect Biol. https://doi.org/10.1101/cshperspect.a032409
20. Paronetto MP, Passacantilli I, Sette C (2016) Alternative splicing and cell survival: from tissue homeostasis to disease. Cell Death Differ 23(12):1919. https://doi.org/10.1038/CDD.2016.91
21. Montero-Hidalgo AJ et al (2023) Alternative splicing in bladder cancer: potential strategies for cancer diagnosis, prognosis, and treatment. Wiley Interdiscip Rev RNA 14(3):e1760. https://doi.org/10.1002/WRNA.1760
22. Pedraza-Arevalo S et al (2023) Spliceosomic dysregulation unveils NOVA1 as a candidate actionable therapeutic target in pancreatic neuroendocrine tumors. Transl Res 251:63–73. https://doi.org/10.1016/j.trsl.2022.07.005

23. Gahete MD, Herman-Sanchez N, Fuentes-Fayos AC, Lopez-Canovas JL, Luque RM, Gahete MD (2022) Dysregulation of splicing variants and spliceosome components in breast cancer. Endocr Relat Cancer 29(9):R123–R142. https://doi.org/10.1530/ERC-22-0019
24. Hermán-Sánchez N, G-García ME, Jiménez-Vacas JM, Yubero-Serrano EM, López-Sánchez LM, Romero-Martín S, Raya-Povedano JL, Álvarez-Benito M, Castaño JP, Luque RM, Gahete MD (2024) The splicing machinery is dysregulated and represents a therapeutic vulnerability in breast cancer. Cell Mol Life Sci. 82(1):18. https://doi.org/10.1007/s00018-024-05515-6
25. Jiménez-Vacas JM et al (2023) Tumor suppressor role of RBM22 in prostate cancer acting as a dual-factor regulating alternative splicing and transcription of key oncogenic genes. Transl Res 253:68–79. https://doi.org/10.1016/j.trsl.2022.08.016
26. Jiménez-Vacas JM et al (2019) Spliceosome component SF3B1 as novel prognostic biomarker and therapeutic target for prostate cancer. Transl Res 212:89–103. https://doi.org/10.1016/j.trsl.2019.07.001
27. Paschalis A et al (2018) Alternative splicing in prostate cancer. Nat Rev Clin Oncol 15(11):663–675. https://doi.org/10.1038/s41571-018-0085-0
28. Del Río-Moreno M et al (2019) Dysregulation of the splicing machinery is associated to the development of nonalcoholic fatty liver disease. J Clin Endocrinol Metab 104(8):3389–3402. https://doi.org/10.1210/JC.2019-00021
29. López-Cánovas JL et al (2023) PRPF8 increases the aggressiveness of hepatocellular carcinoma by regulating FAK/AKT pathway via fibronectin 1 splicing. Exp Mol Med 55(1):132. https://doi.org/10.1038/S12276-022-00917-7
30. López-Cánovas JL et al (2022) Spliceosomal profiling identifies EIF4A3 as a novel oncogene in hepatocellular carcinoma acting through the modulation of FGFR4 splicing. Clin Transl Med. https://doi.org/10.1002/CTM2.1102
31. Delgado ML et al (2024) Splicing Machinery Is Impaired in Oral Squamous Cell Carcinomas and Linked to Key Pathophysiological Features. Int J Mol Sci 25(13):6929. https://doi.org/10.3390/IJMS25136929
32. Vázquez-Borrego MC et al (2019) Splicing machinery is dysregulated in pituitary neuroendocrine tumors and is associated with aggressiveness features. Cancers (Basel). https://doi.org/10.3390/cancers11101439
33. Fuentes-Fayos AC et al (2020) Splicing machinery dysregulation drives glioblastoma development/aggressiveness: oncogenic role of SRSF3. Brain 143(11):3273–3293. https://doi.org/10.1093/brain/awaa273
34. Fuentes-Fayos AC et al (2022) SF3B1 inhibition disrupts malignancy and prolongs survival in glioblastoma patients through BCL2L1 splicing and mTOR/ß-catenin pathways imbalances. J Exp Clin Cancer Res 41(1):1–23. https://doi.org/10.1186/S13046-022-02241-4
35. Bénard J, Douc-Rasy S, Ahomadegbe JC (2003) TP53 family members and human cancers. Hum Mutat 21(3):182–191. https://doi.org/10.1002/HUMU.10172
36. al, "p63, a p53 Homolog at 3q27–29, Encodes Multiple Products with Transactivating, Death-Inducing, and Dominant-Negative Activities," Mol Cell, vol 2, pp 305–316, 1998
37. Momota H et al (2003) Immunohistochemical analysis of the p53 family members in human craniopharyngiomas. Brain Tumor Pathol 20:73–77. https://doi.org/10.1007/s10014-003-0141-y
38. Kim JH et al (2021) In-depth proteomic profiling captures subtype-specific features of craniopharyngiomas. Sci Rep 11(1):1–13. https://doi.org/10.1038/s41598-021-00483-4
39. Apps JR et al (2018) Tumour compartment transcriptomics demonstrates the activation of inflammatory and odontogenic programmes in human adamantinomatous craniopharyngioma and identifies the MAPK/ERK pathway as a novel therapeutic target. Acta Neuropathol 135(5):757–777. https://doi.org/10.1007/S00401-018-1830-2
40. Debnath P, Huirem RS, Dutta P, Palchaudhuri S (2021) Epithelial-mesenchymal transition and its transcription factors. Biosci Rep. https://doi.org/10.1042/BSR20211754
41. Croker BA, Kiu H, Nicholson SE (2008) SOCS regulation of the JAK/STAT signalling pathway. Semin Cell Dev Biol. https://doi.org/10.1016/j.semcdb.2008.07.010
42. Wu S, Du Y, Beckford J, Alachkar H (2018) Upregulation of the EMT marker vimentin is associated with poor clinical outcome in acute myeloid leukemia. J Transl Med 16(1):1–9. https://doi.org/10.1186/S12967-018-1539-Y/FIGURES/7
43. Dang CV (1999) c-Myc target genes involved in cell growth. Mol Cell Biol 19(1):1–11
44. Takeda N et al (2004) Endothelial PAS domain protein 1 gene promotes angiogenesis through the transactivation of both vascular endothelial growth factor and its receptor, Flt-1. Circ Res 95(2):146–153. https://doi.org/10.1161/01.RES.0000134920.10128.B4/FORMAT/EPUB
45. Matsuda T et al (2024) Deciphering craniopharyngioma subtypes: Single-cell analysis of tumor microenvironment and immune networks. iScience 27(11):111068. https://doi.org/10.1016/J.ISCI.2024.111068
46. Garcia-Lavandeira M et al (2012) Craniopharyngiomas express embryonic stem cell markers (SOX2, OCT4, KLF4, and SOX9) as pituitary stem cells but do not coexpress RET/GFRA3 receptors. J Clin Endocrinol Metab. https://doi.org/10.1210/JC.2011-2187
47. Ortiz Torres M, Shafiq I, Mesfin FB (2021) Craniopharyngioma. StatPearls Publishing
48. Dunn J et al (2019) Proteomic analysis discovers the differential expression of novel proteins and phosphoproteins in meningioma including NEK9, HK2 and SET and deregulation of RNA metabolism. EBioMedicine 40:77–91. https://doi.org/10.1016/j.ebiom.2018.12.048
49. Venkataramany AS et al (2022) Alternative RNA splicing defects in pediatric cancers: new insights in tumorigenesis and potential therapeutic vulnerabilities. Ann Oncol 33(6):578–592. https://doi.org/10.1016/J.ANNONC.2022.03.011
50. Jin B et al (2023) MEN1 is a regulator of alternative splicing and prevents R-loop-induced genome instability through suppression of RNA polymerase II elongation. Nucleic Acids Res. https://doi.org/10.1093/nar/gkad548
51. Jiménez-Vacas JM et al (2020) Dysregulation of the splicing machinery is directly associated to aggressiveness of prostate cancer: SNRNP200, SRSF3 and SRRM1 as novel therapeutic targets for prostate cancer. EBioMedicine. https://doi.org/10.1016/j.ebiom.2019.11.008
52. Nikom D, Zheng S (2023) Alternative splicing in neurodegenerative disease and the promise of RNA therapies. Nat Rev Neurosci 24(8):457–473. https://doi.org/10.1038/S41583-023-00717-6
53. Alors-Pérez E et al (2023) Splicing alterations in pancreatic ductal adenocarcinoma: a new molecular landscape with translational potential. J Exp Clin Cancer Res 42(1):1–16. https://doi.org/10.1186/S13046-023-02858-Z/FIGURES/3
54. Blázquez-Encinas R et al (2023) Altered splicing machinery in lung carcinoids unveils NOVA1, PRPF8 and SRSF10 as novel candidates to understand tumor biology and expand biomarker discovery. J Transl Med 21(1):1–16. https://doi.org/10.1186/S12967-023-04754-8/FIGURES/5
55. Jiménez-Vacas JM et al (2020) Dysregulation of the splicing machinery is directly associated to aggressiveness of prostate cancer. EBioMedicine. https://doi.org/10.1016/j.ebiom.2019.11.008
56. Zammarchi F et al (2011) Antitumorigenic potential of STAT3 alternative splicing modulation. Proc Natl Acad Sci. https://doi.org/10.1073/pnas.1108482108
57. Achour C, Prasad Bhattarai D, Groza P, Román Á-C, Aguilo F (2023) ARTICLE OPEN METTL3 regulates breast cancer-associated alternative splicing switches. Oncogene. https://doi.org/10.1038/s41388-023-02602-z
58. Zovoilis A et al (2014) The expression level of small non-coding RNAs derived from the first exon of protein-coding genes is predictive of cancer status. EMBO Rep 15(4):402–410. https://doi.org/10.1002/EMBR.201337950
59. Alexander A, Herz J, Calvier L (2023) Reelin through the years: from brain development to inflammation. Cell Rep. https://doi.org/10.1016/j.celrep.2023.112669
60. Xu Y et al (2023) Clathrin light chain A facilitates small extracellular vesicle uptake to promote hepatocellular carcinoma progression. Hepatol Int. https://doi.org/10.1007/S12072-023-10562-5
61. Labrecque MP et al (2021) RNA splicing factors SRRM3 and SRRM4 distinguish molecular phenotypes of castration-resistant neuroendocrine prostate cancer. Cancer Res 81(18):4736. https://doi.org/10.1158/0008-5472.CAN-21-0307
62. Yu C et al (2019) Characterization of the prognostic values of the NDRG family in gastric cancer. Therap Adv Gastroenterol. https://doi.org/10.1177/1756284819858507
63. Zhou X, Khan S, Huang D, Li L (2022) V-Set and immunoglobulin domain containing (VSIG) proteins as emerging immune checkpoint

targets for cancer immunotherapy. Front Immunol. https://doi.org/10.3389/FIMMU.2022.938470
64. Lang L et al (2023) Adaptive c-Met-PLXDC2 signaling axis mediates cancer stem cell plasticity to confer radioresistance-associated aggressiveness in head and neck cancer. Cancer Res Commun 3(4):659. https://doi.org/10.1158/2767-9764.CRC-22-0289
65. Khalil MI et al (2023) HPV upregulates MARCHF8 ubiquitin ligase and inhibits apoptosis by degrading the death receptors in head and neck cancer. PLoS Pathog. https://doi.org/10.1371/JOURNAL.PPAT.1011171
66. Zhao Y et al (2022) DGKZ promotes TGFβ signaling pathway and metastasis in triple-negative breast cancer by suppressing lipid raft-dependent endocytosis of TGFβR2. Cell Death Dis. https://doi.org/10.1038/S41419-022-04537-X
67. Zhang S et al (2022) GIT1 protects against breast cancer growth through negative regulation of Notch. Nat Commun. https://doi.org/10.1038/S41467-022-28631-Y
68. Qu M et al (2022) Sonic hedgehog signaling: alternative splicing and pathogenic role in medulloblastoma. Genes Dis 10(5):2013. https://doi.org/10.1016/J.GENDIS.2022.10.014
69. Serbis A et al (2023) Predictive factors for pediatric craniopharyngioma recurrence: an extensive narrative review. Diagnostics (Basel). https://doi.org/10.3390/DIAGNOSTICS13091588
70. Macaeva E et al (2016) Radiation-induced alternative transcription and splicing events and their applicability to practical biodosimetry. Sci Rep. https://doi.org/10.1038/SREP19251
71. Zanoni M et al (2022) Irradiation causes senescence, ATP release, and P2X7 receptor isoform switch in glioblastoma. Cell Death Dis. https://doi.org/10.1038/S41419-022-04526-0
72. Moszczyńska E, Prokop-Piotrkowska M, Bogusz-Wójcik A, Grajkowska W, Szymańska S, Szalecki M (2020) Ki67 as a prognostic factor of craniopharyngioma's recurrence in paediatric population. Child's Nerv Syst 36(7):1461. https://doi.org/10.1007/S00381-020-04519-4
73. Saeed H, Leibowitz BJ, Zhang L, Yu J (2023) Targeting Myc-driven stress addiction in colorectal cancer. Drug Resist Updates. https://doi.org/10.1016/j.drup.2023.100963
74. Tang W et al (2022) The miR-3648/FRAT1-FRAT2/c-Myc negative feedback loop modulates the metastasis and invasion of gastric cancer cells. Oncogene. https://doi.org/10.1038/s41388-022-02451-2
75. Miller I et al (2018) Ki67 is a graded rather than a binary marker of proliferation versus quiescence. Cell Rep 24(5):1105. https://doi.org/10.1016/J.CELREP.2018.06.110
76. Sun X, Kaufman PD (2018) Ki-67: more than a proliferation marker. Chromosoma 127(2):175. https://doi.org/10.1007/S00412-018-0659-8
77. Sobecki M et al (2017) Cell-cycle regulation accounts for variability in Ki-67 expression levels. Cancer Res 77(10):2722–2734. https://doi.org/10.1158/0008-5472.CAN-16-0707
78. Kurtovic-Kozaric A et al (2015) PRPF8 defects cause missplicing in myeloid malignancies. Leukemia 29(1):126. https://doi.org/10.1038/LEU.2014.144
79. Prescher N, Hänsch S, Knobbe-Thomsen CB, Stühler K, Poschmann G (2021) The migration behavior of human glioblastoma cells is influenced by the redox-sensitive human macrophage capping protein CAPG. Free Radic Biol Med 167:81–93. https://doi.org/10.1016/J.FREERADBIOMED.2021.02.038
80. Alors-Pérez E et al (2024) Spliceosomic dysregulation in pancreatic cancer uncovers splicing factors PRPF8 and RBMX as novel candidate actionable targets. Mol Oncol. https://doi.org/10.1002/1878-0261.13658
81. Xu Q, Deng B, Li M, Chen Y, Zhuan L (2020) circRNA-UBAP2 promotes the proliferation and inhibits apoptosis of ovarian cancer though miR-382–5p/PRPF8 axis. J Ovarian Res. https://doi.org/10.1186/S13048-020-00685-W
82. Martelli C et al (2019) Investigating the protein signature of adamantinomatous craniopharyngioma pediatric brain tumor tissue: towards the comprehension of its aggressive behavior. Dis Mark. https://doi.org/10.1155/2019/3609789
83. Lindemann C, Hackmann O, Delic S, Schmidt N, Reifenberger G, Riemenschneider MJ (2011) SOCS3 promoter methylation is mutually exclusive to EGFR amplification in gliomas and promotes glioma cell invasion through STAT3 and FAK activation. Acta Neuropathol. https://doi.org/10.1007/s00401-011-0832-0
84. Park AK, Kim P, Ballester LY, Esquenazi Y, Zhao Z (2019) Subtype-specific signaling pathways and genomic aberrations associated with prognosis of glioblastoma. Neuro Oncol 21(1):59. https://doi.org/10.1093/NEUONC/NOY120
85. Henrik Heiland D et al (2019) Tumor-associated reactive astrocytes aid the evolution of immunosuppressive environment in glioblastoma. Nat Commun. https://doi.org/10.1038/S41467-019-10493-6
86. Gao Q et al (2022) Integrative analyses identify HIF-1α as a potential protective role with immune cell infiltration in adamantinomatous craniopharyngioma. Front Immunol. https://doi.org/10.3389/FIMMU.2022.949509/FULL
87. Vidal S, Kovacs K, Lloyd RV, Meyer FB, Scheithauer BW (2002) Angiogenesis in patients with craniopharyngiomas: correlation with treatment and outcome. Cancer 94(3):738–745. https://doi.org/10.1002/CNCR.10281
88. Xu J, Zhang S, You C, Wang X, Zhou Q (2006) Microvascular density and vascular endothelial growth factor have little correlation with prognosis of craniopharyngioma. Surg Neurol 66:S30–S34. https://doi.org/10.1016/J.SURNEU.2006.05.047
89. Qi ST, Zhou J, Pan J, Zhang C, Silky C, Yan XR (2012) Epithelial–mesenchymal transition and clinicopathological correlation in craniopharyngioma. Histopathology 61(4):711–725. https://doi.org/10.1111/J.1365-2559.2012.04297.X
90. Chen M, Zheng SH, Liu Y, Shi J, Qi ST (2016) Periostin activates pathways involved in epithelial-mesenchymal transition in adamantinomatous craniopharyngioma. J Neurol Sci 360:49–54. https://doi.org/10.1016/j.jns.2015.11.042
91. Jia Y et al (2022) Immune infiltration in aggressive papillary craniopharyngioma: high infiltration but low action. Front Immunol. https://doi.org/10.3389/FIMMU.2022.995655
92. Donson AM et al (2017) Molecular analyses reveal inflammatory mediators in the solid component and cyst fluid of human adamantinomatous craniopharyngioma. J Neuropathol Exp Neurol 76(9):779. https://doi.org/10.1093/JNEN/NLX061
93. Zhou J, Zhang C, Pan J, Chen L, Qi ST (2017) Interleukin-6 induces an epithelial-mesenchymal transition phenotype in human adamantinomatous craniopharyngioma cells and promotes tumor cell migration. Mol Med Rep 15(6):4123. https://doi.org/10.3892/MMR.2017.6538
94. Mori M, Takeshima H, Ichi Kuratsu J (2004) Expression of interleukin-6 in human craniopharyngiomas: a possible inducer of tumor-associated inflammation. Int J Mol Med 14(4):505–509. https://doi.org/10.3892/IJMM.14.4.505/HTML
95. An NF-κB signature predicts low-grade glioma prognosis: a precision medicine approach based on patient-derived stem cells, IGA Technology Services Srl, (2018) 20(6): 776–787 https://doi.org/10.1093/neuonc/nox234
96. Zhou L et al (2020) PI3K/AKT signaling pathway mediates the proliferation, migration and invasion of papillary craniopharyngioma cells, https://doi.org/10.21203/RS.3.RS-119581/V2
97. Apps JR et al (2024) Recurrent adamantinomatous craniopharyngiomas show MAPK pathway activation, clonal evolution and rare TP53-loss-mediated malignant progression. Acta Neuropathol Commun. https://doi.org/10.1186/S40478-024-01838-4
98. Alors-Perez E et al (2021) Dysregulated splicing factor SF3B1 unveils a dual therapeutic vulnerability to target pancreatic cancer cells and cancer stem cells with an anti-splicing drug. J Exp Clin Cancer Res. https://doi.org/10.1186/S13046-021-02153-9
99. López-Cánovas JL et al (2021) Splicing factor SF3B1 is overexpressed and implicated in the aggressiveness and survival of hepatocellular carcinoma. Cancer Lett 496:72–83. https://doi.org/10.1016/j.canlet.2020.10.010
100. Venegas-Moreno E et al (2018) Association between dopamine and somatostatin receptor expression and pharmacological response to somatostatin analogues in acromegaly. J Cell Mol Med 22(3):1640. https://doi.org/10.1111/JCMM.13440
101. Vazquez-Borrego MC et al (2020) A somatostatin receptor subtype-3 (SST3) peptide agonist shows antitumor effects in experimental models of nonfunctioning pituitary tumors. Clin Cancer Res 26(4):957–969
102. Luque RM et al (2015) Truncated somatostatin receptor variant sst5TMD4 confers aggressive features (proliferation, invasion and

reduced octreotide response) to somatotropinomas. Cancer Lett 359(2):299–306. https://doi.org/10.1016/j.canlet.2015.01.037
103. Fuentes-Fayos AC et al (2023) Metformin and simvastatin exert additive antitumour effects in glioblastoma via senescence-state: clinical and translational evidence. EBioMedicine 90:104484. https://doi.org/10.1016/j.ebiom.2023.104484
104. Porcel-Pastrana F, Montero-Hidalgo AJ, G-García ME, Gil-Duque I, Prats-Escribano A, Gahete MD, Sarmento-Cabral A, Luque RM, León-González AJ (2025) Cellular and molecular evidence of the synergistic antitumour effects of hydroxytyrosol and metformin in prostate cancer. Int J Mol Sci. 26(3):1341. https://doi.org/10.3390/ijms26031341
105. Dobin A et al (2013) STAR: ultrafast universal RNA-seq aligner. Bioinformatics 29(1):15–21. https://doi.org/10.1093/BIOINFORMATICS/BTS635
106. Hartley SW, Mullikin JC (2016) Detection and visualization of differential splicing in RNA-Seq data with JunctionSeq. Nucleic Acids Res 44(15):e127. https://doi.org/10.1093/NAR/GKW501
107. Li H et al (2009) The Sequence Alignment/Map format and SAMtools. Bioinformatics 25(16):2078. https://doi.org/10.1093/BIOINFORMATICS/BTP352
108. Liao Y, Smyth GK, Shi W (2014) featureCounts: an efficient general purpose program for assigning sequence reads to genomic features. Bioinformatics 30(7):923–930. https://doi.org/10.1093/BIOINFORMATICS/BTT656
109. Robinson MD, McCarthy DJ, Smyth GK (2010) edgeR: a Bioconductor package for differential expression analysis of digital gene expression data. Bioinformatics 26(1):139–140. https://doi.org/10.1093/BIOINFORMATICS/BTP616
110. Trincado JL et al (2018) SUPPA2: Fast, accurate, and uncertainty-aware differential splicing analysis across multiple conditions. Genome Biol 19(1):1–11. https://doi.org/10.1186/S13059-018-1417-1/FIGURES/4

Publisher's Note